NUREG/CR-0839

STUDY OF THERMAL AND HYDRODYNAMIC PROCESSES ASSOCIATED WITH MELTING OF HORIZONTAL SUBSTRATE

Keveh Taghavi-Tafreshi
Vijay K. Dhir

Principal Investigators:
I. Catton
W. E. Kastenberg

School of Engineering and Applied Science
University of California at Los Angeles

Prepared for
U. S. Nuclear Regulatory Commission

Available from
National Technical Information Service
Springfield, Virginia 22161.

NUREG/CR-0839
R7

STUDY OF THERMAL AND HYDRODYNAMIC PROCESSES ASSOCIATED WITH MELTING OF HORIZONTAL SUBSTRATE

Kaveh Taghavi-Tafreshi
Vijay K. Dhir

Principle Investigators:
I. Catton
W. E. Kastenberg

Manuscript Completed: December 1978
Date Published: May 1979

School of Engineering and Applied Science
University of California at Los Angeles
Los Angeles, CA 90024

Division of Reactor Safety Research
Office of Nuclear Regulatory Research
U.S. Nuclear Regulatory Commission
Under Contract No. NRC-04-76-246
NRC FIN NO. B3019

PREFACE

This report represents one aspect of the research program "Safety" Considerations of Commercial Liquid Metal Fast Breeder Reactors," AT(04-3) PA223, AT(49-24)-0246 and NRC(04-76-246) funded by the U. S. Nuclear Regulatory Commission, Office of Nuclear Regulatory Research, Division of Reactor Safety Research. The research program is divided into the following tasks: (a) transient analysis of fuel elements, (b) accident analysis, (c) post-accident heat removal, (d) fuel-coolant interactions, and (e) thermodynamic effects.

Reports prepared previously under this grant include the following:

1. Post Accident Heat Removal with Advanced LMFBR Fuels, R.D. Gasser, UCLA-ENG-7518 (March 1975).
2. Dry-Out of a Fluidized Particle Bed with Internal Heat Generation, R. S. Keowen and I. Catton, UCLA-ENG-7519 (March 1975).
3. Laminar Natural Convection from Blunt Bodies with Arbitrary Surface Heat Flux or Surface Temperature, G. M. Harpole, UCLA-ENG-7527 (April 1975).
4. Preliminary Assessments of Carbide Fuel Pins during Mild Overpower Transients, G. M. Nickerson, UCLA-ENG-7582 (October 1975).
5. A Simplified Method of Computing Clad and Fuel Strain and Stress during Irradiation, Y. Sun and D. Okrent, UCLA-ENG-7591 (Part I) (October 1975).
6. An Experimental Study of the Thermal Interaction for Molten Tin Dropped into Water, V. M. Arakeri, I. Catton, W. E. Kastenberg, and M. S. Plesset, UCLA-ENG-7592 (December 1975).

7. A Mechanistic Study of Fuel Freezing and Channel Plugging during fast Reactor Overpower Excursions, V. K. Dhir, K. W. Wong, and W. E. Kastenberg, UCLA-ENG-7679 (July 1976).

8. A Simulation of Thermal Phenomenon Expected in Fuel Coolant Interactions in LMFBR's, J. Yasin, NUREG-0187 (September 1976).

9. On the Nonequilibrium Behavior of Fission Gas Bubbles with Emphasis on the Effects of Equation of State, W. G. Steele, NUREG-0186 (December 1976).

10. A Method for the Determination of the Equation of State of Advanced Fuels Based on the Properties of Normal Fluids, M. J. Hecht, NUREG-0177 (December 1976).

11. A Simplified Method of Computing Clad and Fuel Strain and Stress During Irradiation, Y. Sun and D. Okrent, NUREG-0260 (Part II) (January 1977).

12. Natural Convection in Horizontal Fluid Layers, A. J. Suo-Anttila and I. Catton, NUREG-0261 (January 1977).

13. An Experimental Study of the Molten Glass/Water Thermal Interaction under Free and Forced Conditions, V. H. Arakeri, I. Catton, and W. E. Kastenberg, NUREG-0263 (January 1977).

14. Study of Dryout Heat Fluxes in Beds of Inductively Heated Particles, V. K. Dhir and I. Catton, NUREG-0262 (February 1977).

15. A Look at Alternate Core Disruption Accidents in LMFBR's, C. K. Chan, T. K. Min, and D. Okrent, NUREG-0259 (February 1977).

16. A Mechanistic Study of Fuel Freezing, Channel Plugging, and Continued Coolability During Fast Reactor Overpower Excursions, K. W. Wong, NUREG-0310 (July 1977).

17. Natural Convection Heat Transfer in Beds of Inductively Heated Particles, S. J. Rhee and V. K. Dhir, NUREG-0408 (September 1978).

TABLE OF CONTENTS

NOMENCLATURE

C	=	constant
c_p	=	specific heat
g	=	gravitational acceleration
h	=	heat transfer coefficient
h_{sf}	=	latent heat of fusion
h'_{sf}	=	latent heat of fusion corrected for sensible heat, $h_{sf}\ (1 + c_{po}\ \Delta T/2h_{sf})$
h_{sg}	=	latent heat of vaporization
	=	thermal conductivity
$\overset{o}{m}''$	=	mass flux
q	=	heat flux
R	=	droplet radius
r	=	radius
Re	=	Reynolds number, $q\lambda/\mu_g h_{sg}$
T	=	temperature
t	=	time
$\bar{u}$	=	mean film velocity in the radial direction
V	=	droplet volume
v	=	velocity in the vertical direction
Δp	=	pressure difference
ΔT	=	temperature difference between interface and melting or subliming surface
σ	=	thermal diffusivity of the frozen olive oil
δ	=	film thickness
η	=	droplet height
λ	=	wavelength

λ_c, λ_d	=	critical and "most dangerous" wavelength respectively
ω	=	growth rate frequency
μ	=	viscosity
ρ	=	density
σ	=	surface tension between two immiscible fluids

Superscript

*	=	quantities nondimensionalized with $\sqrt{\sigma/g\,(\rho_w - \rho_o)}$

Subscripts

c	=	conduction to slab
f	=	liquid
g	=	gas
i	=	interface
m	=	mean
o	=	liquid olive oil
r	=	raw
s	=	melt surface
se	=	sensible heat to olive oil
t	=	total
w	=	water
∞	=	initial frozen olive oil slab temperature

LIST OF FIGURES

LIST OF TABLES

ACKNOWLEDGMENT

Financial support provided by the Reactor Safety Research Division of the U.S. Nuclear Regulatory Commission under Contract No. NRC-04-76-246 is greatfully acknowledged.

ABSTRACT OF THE REPORT

Study of Thermal and Hydrodynamic Processes
Associated with Melting of Horizontal Substrate

by

Kaveh Taghavi-Tafreshi

Vijay K. Dhir

School of Engineering and Applied Science
University of California
Los Angeles, California

The melting of a horizontal slab of frozen olive oil placed beneath a pool of warm water has been studied experimentally. The interfacial heat flux data are taken in quasi-static mode by noting the time rate change of enthalpy of the pool of water. Because of little agitation of the pool due to low melt volume flux (ρ_w/ρ_o = 1.09; ΔT = 5 - 45 K), the pool was found to stratify with time. Hence, heat transfer coefficient data have been based on both the mean pool temperature and the interfacial temperature. Visual observations show that melt removal is governed by Taylor instability and that melt releasing nodes lie about a Taylor wavelength apart. Predictions of the interface growth based on equilibrium between surface tension and buoyant forces have been made and found to compare well with the data obtained from the movies. The heat transfer coefficient data obtained at higher pool

temperatures are also predicted well by the theoretical model.

I. INTRODUCTION

The aim of the present study is to show how Taylor instability may govern the heat transfer from a liquid pool to a melting horizontal surface lying underneath, when the melt density is less than the density of the pool. Understanding of such a physical process is essential to obtain better evaluation of certain types of hypothetical accidents in liquid metal fast breeder reactors. In postulating a hypothetical core disruptive accident a scenario may be imagined where a layer of liquid UO_2 is formed on a horizontal steel surface. The removal of molten steel from underneath of denser liquid UO_2 would be governed by Taylor instability as long as a UO_2 crust does not separate liquid UO_2 and steel surface. In this study a situation, where the ratio of the density of the overlaying liquid to the melt density is of the same order as it would be in UO_2 - steel combination, is created by forming a pool of warm water over a slab of frozen olive oil.

Taylor instability has been applied in the past to explain many diverse physical phenomena, such as film boiling, maximum and minimum pool boiling heat fluxes, condensation on the underneath of a flat plate or tube, and so on.

In 1950, Taylor [1][1] discussed the instability of a horizontal interface between two ideal immiscible fluid of infinite depth. He showed that the irregularities at the interface tended to grow if the acceleration was directed from heavier fluid to the less dense fluid. Bellman and Pennington [2] extended Taylor's analysis by taking into

---

[1] Numbers in square brackets represent entries in reference section.

account the interfacial tension and the viscosities of the two fluids. For a simple case in which only surface tension at the interface was considered, they obtained analytical expressions for the fastest growing unstable wavelength and its growth rate.

Zuber [3], in 1959, made the first successful attempt in applying Taylor instability to predict minimum and maximum heat fluxes for pool boiling. He proposed that near the minimum heat flux the bubbles would be released on a square grid with spacing bounded between the fastest growing and critical Taylor wavelengths. Using two dimensional most dangerous and critical wavelengths, and considering that two bubbles were released per cycle per λ^2 area of the heater, and determining bubble growth rate by averaging it over the amplitude, Zuber obtained an expression for the minimum heat flux from purely hydrodynamic consideration.

Subsequently, Berenson [4,5] made several careful observations of the minimum heat fluxes for carbon tetrachloride and pentane boiling on flat plates. Berenson redrived Zuber's expression for the minimum heat flux by restricting the bubble spacing to the fastest growing Taylor wavelength and by determining the average bubble growth rate from experimental data rather than averaging it over the amplitude as Zuber had done originally. However, Berenson kept Zuber's original assumption of a two-dimensional Taylor wave at the interface of two inviscid liquids of infinite depth and a release of two bubbles per cycle per λ^2 area. He also obtained an expression for the film boiling heat transfer coefficient near the minimum by employing an average geometrical model of film boiling process. Combining the expression for the heat transfer coefficient and that of minimum heat flux, he also

obtained an expression for the minimum temperature difference required to sustain film boiling.

In the earlier studies by Zuber and Berenson no specific reasons were given for choosing a two dimensional Taylor wavelength over the more logical three dimensional one. Subsequently, Sernas, et. al. [6] showed that if a 3-dimensional Taylor wavelength is used which is $\sqrt{2}$ times greater than the 2-dimensional wavelength, it will result in four bubbles per λ^2_{3-D} area of the heater. In other words it will yield two bubbles per λ^2_{2-D} area of the heater as had been earlier used by Zuber and Berenson.

Recently, in 1976, Dhir, et. al. [7] studied steady and quasi-static heat transfer from liquid pools of water and benzene to a horizontal slab of dry ice. They observed that as long as a minimum temperature difference existed between dry ice and the overlaying liquid, a stable gas film was separating the two. For pool temperatures above the minimum, the film was called either laminar or turbulent, while for pool temperatures below the minimum, a partial liquid solid contact was assumed to exist. In turbulent film they found the heat transfer coefficient to be strongly dependent on pool temperature and proportional to $Re^{0.5}$. For laminar film they assumed a geometrical model similar to that of Berenson, but based on experimental observations it was assumed that only one bubble per cycle per λ^2 area of the slab was released. Dhir, et. al. argued that heat transfer to the slab at bubble nodes resulted in relatively less sublimination of dry ice at the bubble releasing nodes than the rest of the area. This in turn caused the development of peaks and valleys in the surface. Thereafter, because of negative curvature, the interface in the valleys became more stable

and bubbles continued to be released only at the locations (peaks) which were more susceptible to instability.

The result of this work was the development of an expression for laminar pseudo film boiling heat transfer coefficient.

$$h = 0.36 \left[\frac{k_g^3 h_{sg} g (\rho_\ell - \rho_g) \rho_g}{\mu_g \Delta T \sqrt{\sigma / g(\rho_\ell - \rho_g)}} \right]^{1/4} \quad (1)$$

Equation (1) is similar to that of Berenson but has a numerical constant 15% less than that in Berenson's expression for film boiling on flat plates. Experimental data in reference [7] showed that equation (1) was valid as long as a stable gas film separated the overlaying liquid from the dry ice surface and the film was laminar. However, when the temperature difference across the film was such that a stable film could no longer be maintained, a partial freezing of the overlaying liquid started to occur at the interface. The heat flux quickly dropped to zero as the temperature of the pool approached its freezing temperature. Most of the observations of reference [7] have subsequently been corroborated by Alysmeyer and Reimann [8]. Alysmeyer and Reimann also qualitatively observed melting of frozen benzene and frozen o-xylene under water at about 298 K. They noted that the melting process was indeed governed by Taylor instability even for small density difference between the melt and the overlaying liquid.

While discussing the effects of various system variables on core compaction and recriticality [9], the heat transfer from molten UO_2 to a melting steel surface was envisioned to be controlled by Taylor instability. The magnitude of heat transfer coefficient was obtained from expression (1) by using the properties of molten steel and molten UO_2 to

represent the properties of gas and liquid respectively. Though equation (1) could be expected to yield rough estimates of heat transfer between UO_2 and melting surface, yet equation (1) as applied to UO_2 - steel system had two weaknesses. First, an experimental verification of equation (1) had not been done for a melting process as opposed to a sublimation process. Secondly, the potential of formation of UO_2 crust between molten UO_2 and steel was neither investigated nor the limitations, the formation of crust imposed on equation (1) were ascertained.

In the present work attention has been focused on Taylor instability driven melting process to understand the difference between melting (low density difference between pool and melt) and sublimation (high density difference between pool and gas) process, and how these differences affect equation (1). The melting process with small density difference between pool and melt (immiscible fluids) is expected to be slower as compared to the one where solid surface releases gas as a result of heat transfer. The dominant wavelength in a low density difference melting process should be about the same as in film boiling near critical pressure [10,11]. However, mechanics of the bubble growth and break up in melting and film boiling near the critical pressure would be different, because surface tension and latent heat of vaporization vanish near the critical pressure, whereas in a melting process both have high values.

The heat transfer model for a slowly growing interface is described in Chapter II. The experimental apparatus and procedure used to conduct the melting experiments is described in Chapter III. Results are discussed in Chapter IV. Conclusions are made in Chapter V.

Appendix A lists necessary thermophysical properties of the reagents used in this study. Error analyses are made in Appendix B. Appendix C studies about the effect of olive oil viscosity on the most dangerous wavelength and its growth rate.

II. ANALYSIS

In many respects, the melting of lighter immiscible liquid as a result of heat transfer from a heavier overlying liquid will be similar to pseudo film boiling studied in reference [7]. A liquid film will be formed on the surface of the melting solid from which melt droplets governed by Taylor instability will be released cyclically. Because there is less melting beneath a droplet release node than in the region between two adjacent release nodes, the melt surface will become uneven and a standing wave pattern will be established on the surface. Subsequently, the droplets will be released only from nodes of the wave which coincide with ridges on the surface and no droplet will be released from antinodes of the wave which coincide with valleys on the surface. Droplets are not released from the valley because the interface there becomes relatively stable due to negative curvature. Figure 1 shows the physical model of the melting process.

The melting process will be signif antly slower than pseudo film boiling because of the higher density of the melt phase (relative to a gas film) and much smaller density difference between the overlying pool and the melt. This can easily be seen from the expression of linear interface growth rate between two immiscible, inviscid liquids of infinite depth. The local interface position for the "most dangerous" wavelength can be written as a function of time:

$$\eta = \eta_o e^{\omega_{max} t}, \tag{2}$$

where ω_{max} is the growth frequency of the "fastest" growing Taylor wave and is given as [2]:

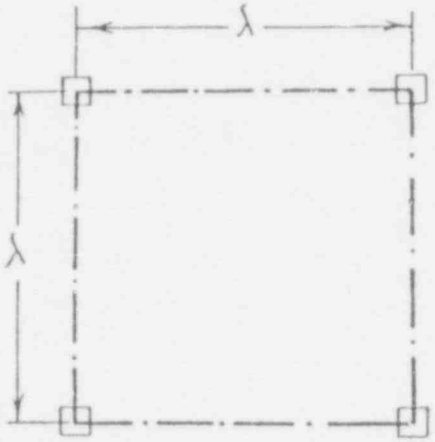

a. Droplet Releasing Nodes at the Melting Surface

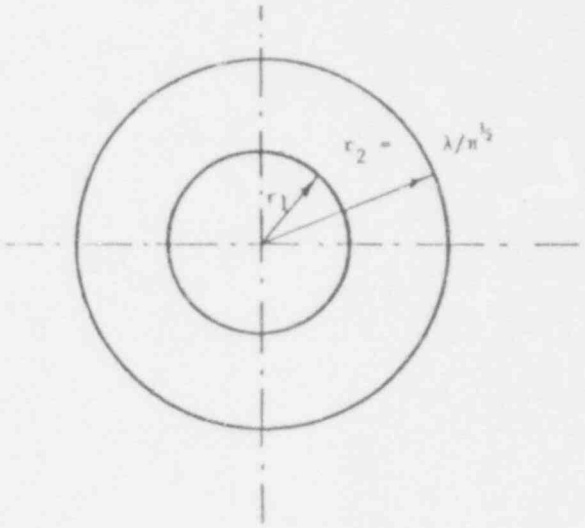

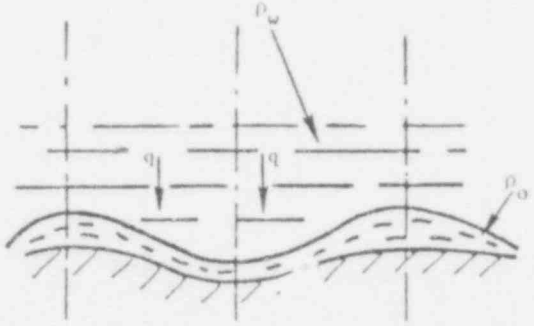

b. Melting Process

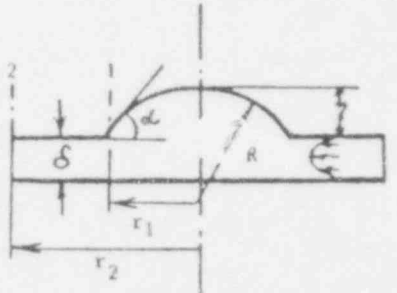

c. Hydrodynamic and Heat Transfer Model

Fig. 1. Physical Model of the Melting Process.

$$\omega_{max} \approx \left\{ \frac{[g(\rho_f - \rho_g)^3]}{\sigma(\rho_f + \rho_g)^2} \right\}^{1/4} \tag{3}$$

The notation here conforms with that of earlier work describing a gas film (g) underlying a liquid fluid (f). The buoyancy tends to move the disturbed interface upward, while surface tension holds it back. As the density of the lighter fluid approaches the heavier liquid, the growth rate would become very small. In this case it may be appropriate to say that, "the liquid-liquid interface moves so slowly that at each quasi-static position of the interface the surface tension force is in equilibrium with the buoyancy force."

Assuming that the growing interface (droplet) is part of a sphere as shown in Figure 1c, the base radius (half chord length) of the droplet can be written in terms of the maximum droplet height and droplet radius as:

$$\begin{aligned} r_1^2 &= R^2 - (R-\eta)^2 \\ &= \eta R(2 - \eta/R) \end{aligned} \tag{4}$$

The droplet volume because

$$V = \pi R \eta^2 (1 - \eta/3R) \tag{5}$$

Equating the buoyant and surface tension forces acting upon an oil droplet in water yields:

$$V(\rho_w - \rho_o)g = 2\pi r_1 \sigma \sin \alpha$$

Substituting for r_1 and V from equations (4) and (5) and noting $\sin \alpha = r_1/\ell$ yields:

$$\pi R \eta^2 (1-\eta/3R)(\rho_w - \rho_o)g = 2\pi \eta \sigma (2-\eta/R)$$

Using $\sqrt{\sigma/g(\rho_w - \rho_o)}$ as a characteristic length, a dimensionless droplet radius can be written in terms of a dimensionless interface height as

$$R^* = \frac{(\eta^{*2}+12) + \sqrt{(\eta^{*2}+12)^2 - 72\eta^{*2}}}{6\eta^*}$$

The dimensionless droplet radius from equation (6) is plotted in Figure 2. In this figure, the dimensionless droplet base radius and dimensionless droplet volumes obtained from equations (4) and (5) respectively are also plotted with R* defined by equation (6). It is observed that droplet radius decreases rapidly with droplet height while the droplet base radius decreases slightly. The droplet radius and base radius become equal at $\eta^* = \sqrt{3}$, when the droplet becomes a hemisphere. The droplet volume increases with * and becomes maximum when $\eta^* \simeq 1.5$. A further increase in droplet height would demand a decrease in droplet volume if equilibrium between buoyant and surface tension forces is to hold. A decrease in droplet volume is not possible in the present process because an increase in droplet height is associated with influx of melt into the droplet. Thus, with additional mass flux the droplet would acquire another shape, which, probably would give it a larger height and a smaller base than dictated by equilibrium condition. This in turn would cause the buoyant force to significantly exceed the surface tension force and the droplet would break away from the interface. Generally, in a cyclical process the droplet will always have some initial volume at the start of the growth period. Thus, through one cycle a droplet will start with some value of $\eta^* > 0$ and terminate with $\eta^* > 1.5$.

Next, to develop a model for the heat transfer, we assume that one droplet is released per λ^2 area per cycle (Fig. 1b) and that this area can be replaced by an equivalent circle of radius r_2 (Fig. 1c) such that

$$r_2 = \lambda/\sqrt{\pi} \tag{7}$$

Also, the center of the base of the droplet coincodes with the center of the equivalent circle. We further assume that

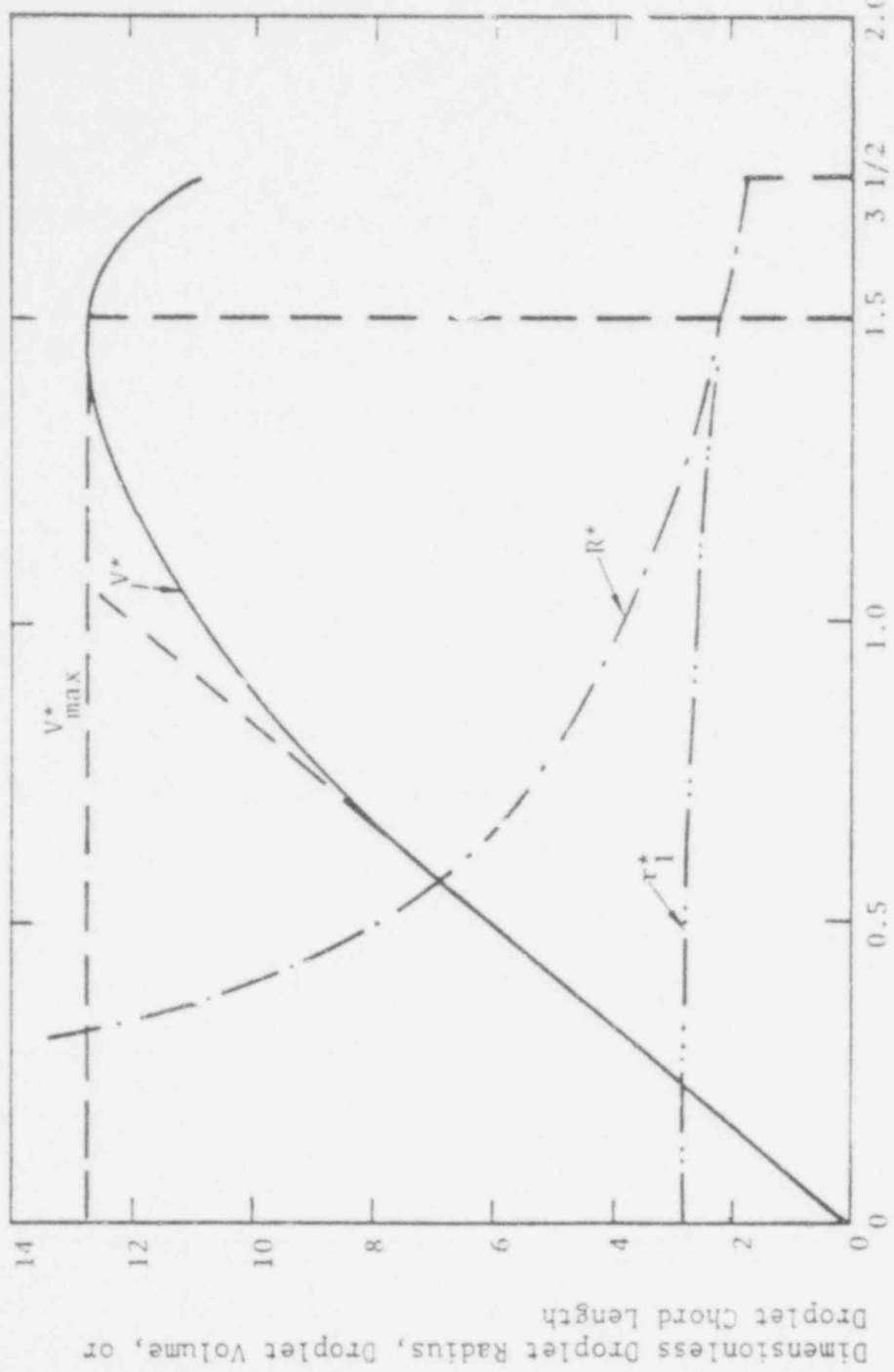

Fig. 2. Dependence of Droplet Volume, Droplet Radius, and Droplet Chord Length on the Interface Height

(i) The olive oil-water interface temperature is approximated to remain constant during a cycle.

(ii) The slab of frozen olive oil is slightly subcooled so that most of the energy is utilized in the phase change and in supplying sensible heat to the melt.

(iii) The oil film is thin and the liquid velocity in the film is small so that inertial forces can be neglected and a linear temperature distribution can be assumed across the film.

(iv) The liquid film is laminar and a no-slip condition exists at both the slab surface and at the interface.

(v) The effect of evolution of melt at the surface of the solid in reducing shear stress and heat transfer is small. The validity of assumptions (iii), (iv) and (v) has been shown in reference [7] for the pseudo film boiling process. These assumptions should also hold for the melting process.

(vi) The melt flows radially into the droplet and does not affect the droplet spacing.

(vii) The melt properties are evaluated at the average film temperature.

For a film of constant thickness δ, a simple energy balance at the interface and an arbitrary radius r, yields the melt velocity in the vertical direction as

$$v = \frac{k_o \Delta T}{\delta \rho_o h'_{sf}} \tag{8}$$

The mean film velocity $\bar{u}$, in the radial direction is related to the vertical velocity v as

$$\rho_o \bar{u} . 2\pi r\delta = \pi(r_2^2 - r^2) v \rho_o$$

or

$$\bar{u}/v = \frac{(r_2^2 - r^2)}{2r\delta} \quad . \tag{9}$$

Substituting in equation (9) for v from equation (8) results in

$$\bar{u} = \frac{k_o \Delta T}{\rho_o h'_{sf}} \frac{r_2^2 - r^2}{2r\delta^2} \tag{10}$$

The radial pressure drop with no slip at the melting surface and at the olive oil interface (Fig. 1c) can be written as

$$\frac{dp}{dr} = \frac{12\mu_o \bar{u}}{\delta^2} \tag{11}$$

Substitution of $\bar{u}$ from equation (10) in equation (11) gives

$$\frac{dp}{dr} = \frac{12\mu_o k_o \Delta T}{\delta^4 \rho_o h'_{sf}} \frac{(r_2^2 - r^2)}{2r} \tag{12}$$

For constant film thickness integration of equation (12) between points 2 ($=r_2$) and 1 ($=r_1$) yields

$$(\Delta p)_{2-1} = \frac{3\mu_o k_o \Delta T}{\delta^4 \rho_o h'_{sf}} \left(2 r_2^2 \ln \frac{r_2}{r_1} + r_1^2 - r_2^2\right) \tag{13}$$

The hydrostatic pressure difference between points 2 and 1 can be written while accounting for the contribution of surface tension as

$$(\Delta p)_{2-1} = (\rho_w - \rho_o) g \eta - 2\sigma/R \tag{14}$$

Elimination of $(\Delta p)_{2-1}$ between equations (13) and (14) yields

$$\delta = \left[C_1 \frac{\mu_o k_o \Delta T \sqrt{\sigma/g(\rho_w - \rho_o)}}{h'_{sf} \rho_o (\rho_w - \rho_o) g} \right]^{1/4} \tag{15}$$

where

$$C_1 = \left[\frac{3(2r^{*2}_2 \ln \frac{r^*_2}{r^*_1} + r^{*2}_1 - r^{*2}_2)}{(\eta^* - 2/R^*)} \right]^{1/4}$$

Once r_2^* is fixed, constant C_1 can be evaluated in terms of η^* while using equation (6) for R^*. Equation (15) for δ has been arrived at by assuming that heat is transferred only through the unit cell area not covered by the droplet and no heat is transferred through the droplet. Thus, to obtain the film thickness which would give an average heat transfer over the unit cell, equation (15) should be multiplied by the ratio of the area of the cell to the area not covered by the droplet. Or

$$\delta = C_1 \left(\frac{r_2^{*2}}{r_2^{*2}-r_1^{*2}}\right) \left[\frac{\mu_o k_o \Delta T \sqrt{\sigma/g(\rho_w-\rho_o)}}{h'_{sf}\rho_o(\rho_w-\rho_o)g}\right] \tag{16}$$

The average heat transfer coefficient over the melting surface can, finally be written as

$$h = \frac{k_o}{\delta} = C\left[\frac{k_o^3 h'_{sf}\rho_o(\rho_w-\rho_o)g}{\mu_o \Delta T\sqrt{\sigma/g(\rho_w-\rho_o)}}\right] \tag{17}$$

where

$$C = \left(\frac{1-r_1^{*2}/r_2^{*2}}{C_1}\right) . \tag{18}$$

The constants C_1 and C are plotted in Figure 3 as a function of η^* for $\lambda = \lambda_d$, $0.8\lambda_d$, and λ_c. This figure shows that film thickness for each wavelength weakly depends on η^* and can be considered nearly constant for η^* between ≈0.4 and 1.5. This observation is of significant importance as it justifies the assumption that film thickness remains constant throughout a droplet cycle. The predicted film is thinnest for the critical wavelength and is thickest for the "most dangerous" wavelength. For $\lambda = \lambda_d$; $0.8\lambda_d$ the constant C - verage heat transfer coefficient increases with η^* until $\eta^* = 1.5$; but for $\lambda = \lambda_c$, it continues to increase up to $\eta^* = \sqrt{3}$. Physically, the rapid change in heat transfer

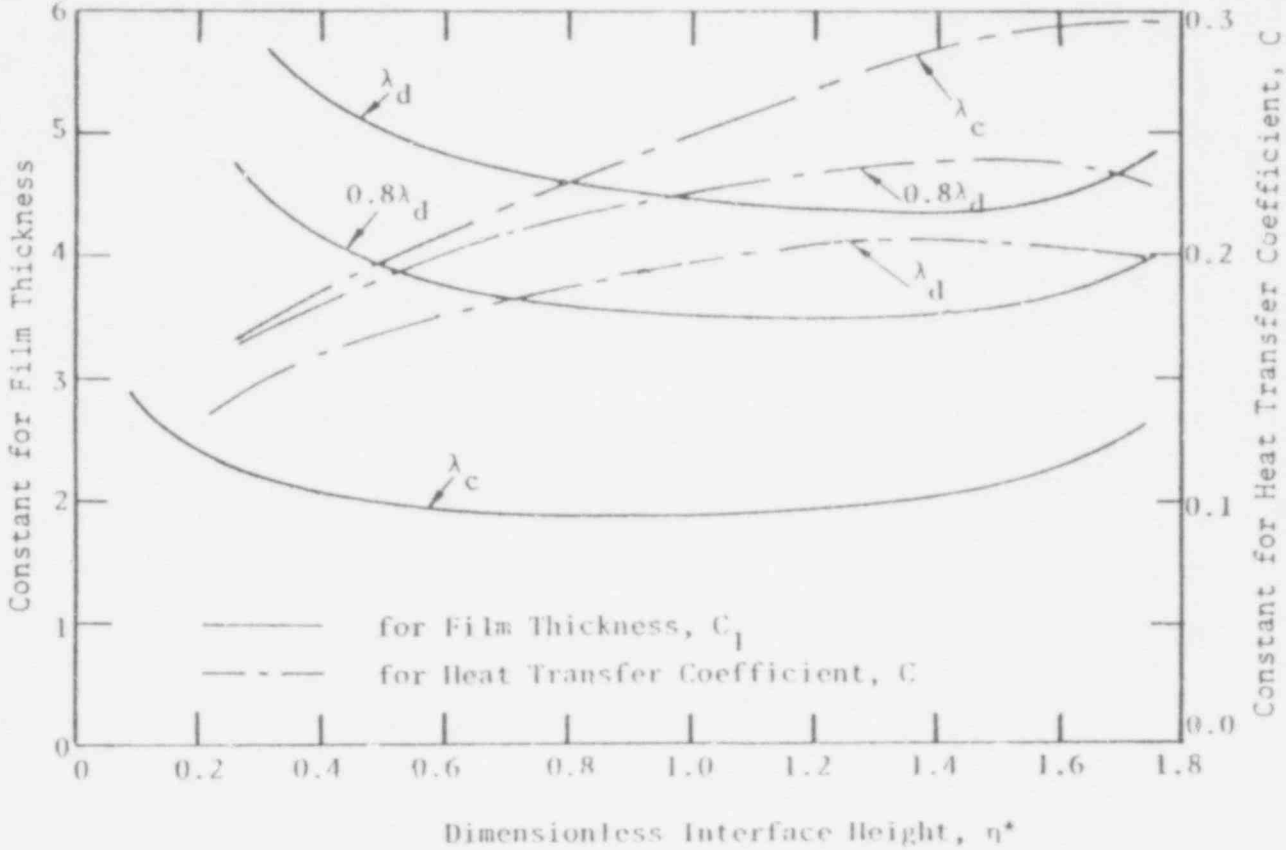

Fig. 3. Dependence of Coefficients of Film Thickness, C_1, and Heat Transfer Coefficient, C, on Interface Height and Wavelength.

during the interface growth period demanded by the critical wavelength may not be possible. Therefore, wavelengths greater than "critical" which give nearly uniform heat transfer rate during the growth period may be preferred. Perturbations most susceptible to growth are ones which give a wavelength close to the fastest growing Taylor wavelength. However, as we see from Figure 3, higher heat transfer occurs for $\lambda = 0.8\lambda_d$. Generally, the process would try to optimize itself and would favor wavelengths which are somewhat shorter than the "most dangerous" wavelength. This predicted behavior is similar to experimental observations made during film boiling of CO_2 near the critical pressure [10]. In film boiling of CO_2 wavelengths between critical and "most dangerous" wavelengths are found to be dominant.

The wavelengths used in plotting the constants C_1 and C are based on viscous, immiscible, and infinite liquid depth assumptions. The effect of liquid viscosity is generally to lengthen the most dangerous wavelength and to reduce the growth rate, however, the most critical wavelength remains unaffected by liquid viscosity [12,13]. Using the general method outlined in reference [2], "most dangerous" wavelengths for olive oil-water combinations was calculated, and 17% increase was observed (Appendix C), though the finite melt layer is not expected to influence much the "most dangerous" wavelength [14]. Now if we assume that during one cycle the interface grows from $\eta^* = 0.3$ (droplet starts with some initial volume) to $\eta^* = 1.5$ and that the dominant wavelength is $0.8\,\lambda_d$, then the average value of constant C is obtained from Figure 3 as 0.22.

III. EXPERIMENTAL APPARATUS AND PROCEDURE

Preliminary experiments were conducted when a 5.0 cm thick layer of frozen olive oil was formed in a 28 cm diameter, and 5.0 cm deep pan made out of a 0.4 cm thick aluminum sheet. Olive oil was frozen by placing the pan in a box containing dry ice slabs. Aluminum was chosen as the material for the pan because of its high thermal conductivity. The liquid pool of frozen olive oil was formed in a 28 cm diameter, 40 cm high, and 0.6 cm thick plexiglas cylinder. Plexigas was chosen because of its relatively low thermal conductivity and good transparency. Smaller thermal conductivity of plexiglas would result in lower heat loss to surroundings. Figure 4 shows the test apparatus. The plexiglas jar and aluminum pan were separated by a rubber gasket and held in place by means of 8 bolts and nuts. A valve was provided at the side wall of the pan to drain out the water after each experiment. To measure the temperature of the frozen slab of olive oil, a sheated chromel-alumel thermocouple was placed in the pan through the drain pipe. The output of the thermocouple was read on a Lead and Northrup potentiameter.

A series of experiments was conducted by forming a pool of warm water over the frozen olive oil slab. In the preliminary experiments both pool temperature and pool height were changed. Although these experiments were not used to obtain quantitative heat transfer data, yet several useful conclusions were made which later helped in designing better experiments. The main observations made from these experiments are listed below:

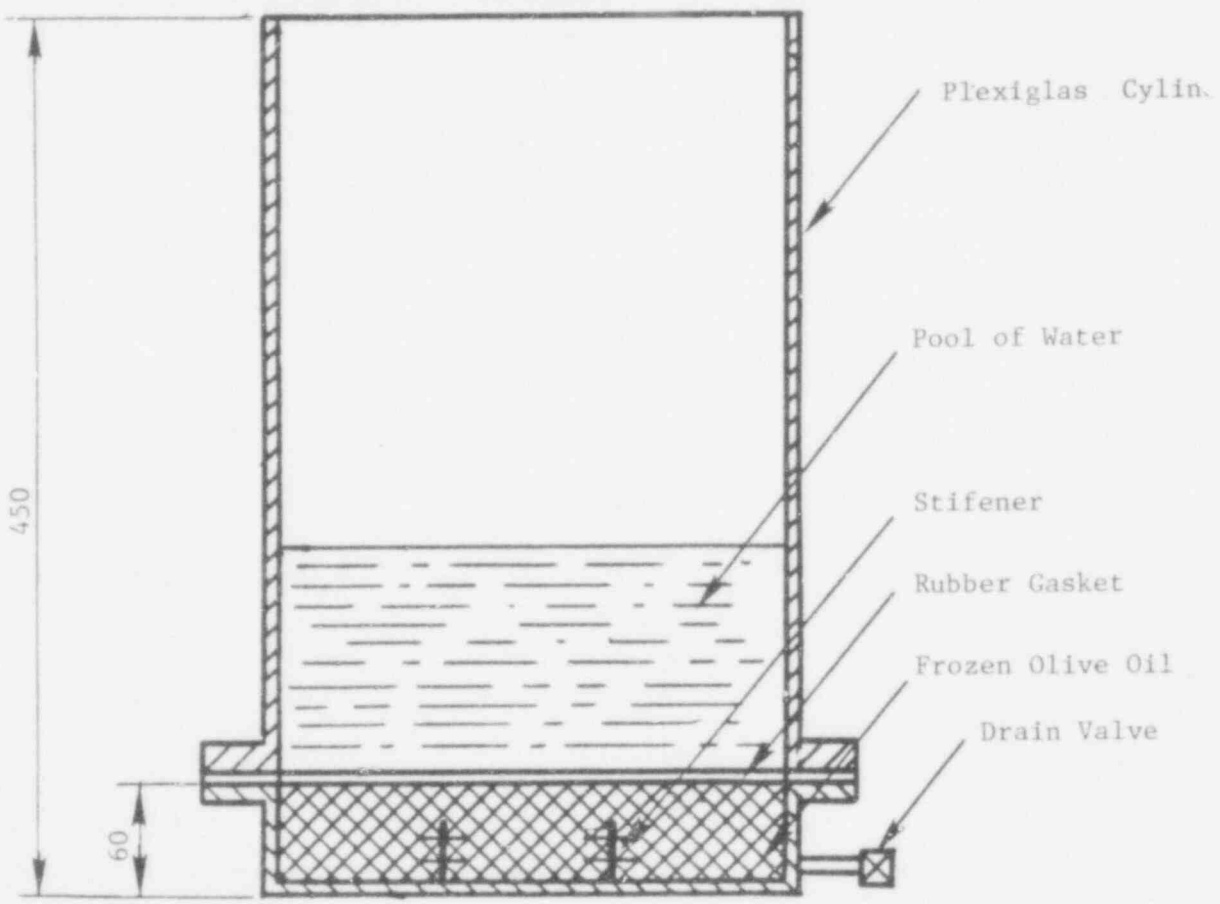

Fig. 4. Preliminary Test Apparatus

(i) Though choice of aluminum pan and dry ice bath reduced preparation time substantially, yet due to the rapid cooling, the frozen olive oil slab was always found to be cracked and the free surface of the slab was hardly ever horizontal. Also, the slab usually was highly subcooled and this subcooling varied from one experiment to another.

(ii) After the pool of warm water was formed over the olive oil slab, heat was axially conducted through the side wall of the plan which in turn resulted in the melting of olive oil slab from the sides even faster than that of the slab free surface.

(iii) Although the water pool was formed in plexiglas jar, good observations of droplet spacing, growth and melt layer thickness could not be made because of the nature of the apparatus.

(iv) Experiments with different pool heights showed that there was no change in the droplet release mechanism as long as the pool was deep enough such that during pinching off from the interface the droplets remained completely in the pool. This minimum pool height was found to be 3 cm.

(v) The observations of temperature distribution in the pool showed that the pool tended to stratify with time.

1. Experimental Apparatus

The above observations helped in designing an improved experimental apparatus. In the later version a 6.5 cm thick layer of olive oil was formed in a 30 cm diameter, 30 cm high, and 0.62 cm thick pyrex jar. Olive oil was frozen by placing the pyrex jar in a refrigerator for several hours. The inside temperature of the refrigerator was found to

. main nearly constant with time and was about 266 K. The use of the refrigerator resulted in slow cooling and perfectly horizontal frozen oil slab with no cracks. The slab, as it was removed from the refrigerator was found to be about 5.5 K subcooled. A 5 cm thick layer of water was formed over the frozen oil slab. As concluded from the preliminary experiments the pool tended to stratify with time. Therefore a thermopile consisting of ten chromel-alumel thermocouples which were located at different height in the pool was formed. The thermocouples were made from 30 gage teflon coated chromel-alumel wires. The thermocouples were passed through 3 mm outer diameter, 30 cm long glass tubes. To reduce the axial heat conduction through the glass tubes and thermocouple beads; the thermocouple wires located in the pool were additionally passed through 1.6 mm diameter, 5 cm long two hole mulite insulators. To hold these glass tubes carrying the thermocouple wires in place, the glass tubes were passed through holes drilled in two aluminum circular discs. The circular discs were mounted on a threaded rod. Fig. 5 shows the thermopile assembly in detail. The thermopile assembly itself was supported on a stand made out of 2.5 cm square aluminum rod. The test apparatus including the thermopile assembly is shown in Figure 6. The thermopile could be moved up and down by turning a nut riding on the threaded rod. Each revolution of the nut resulted in a 1.56 mm vertical movement of the thermopile. To prevent the rotation of the thermopile assembly while the nut was turned, a 3 mm diameter steel rod was passed through the circular discs and through a hole in the stand. Beside the ten thermocouples used to measure pool temperature, the thermopile assembly included two other thermocouples to measure the temperature at

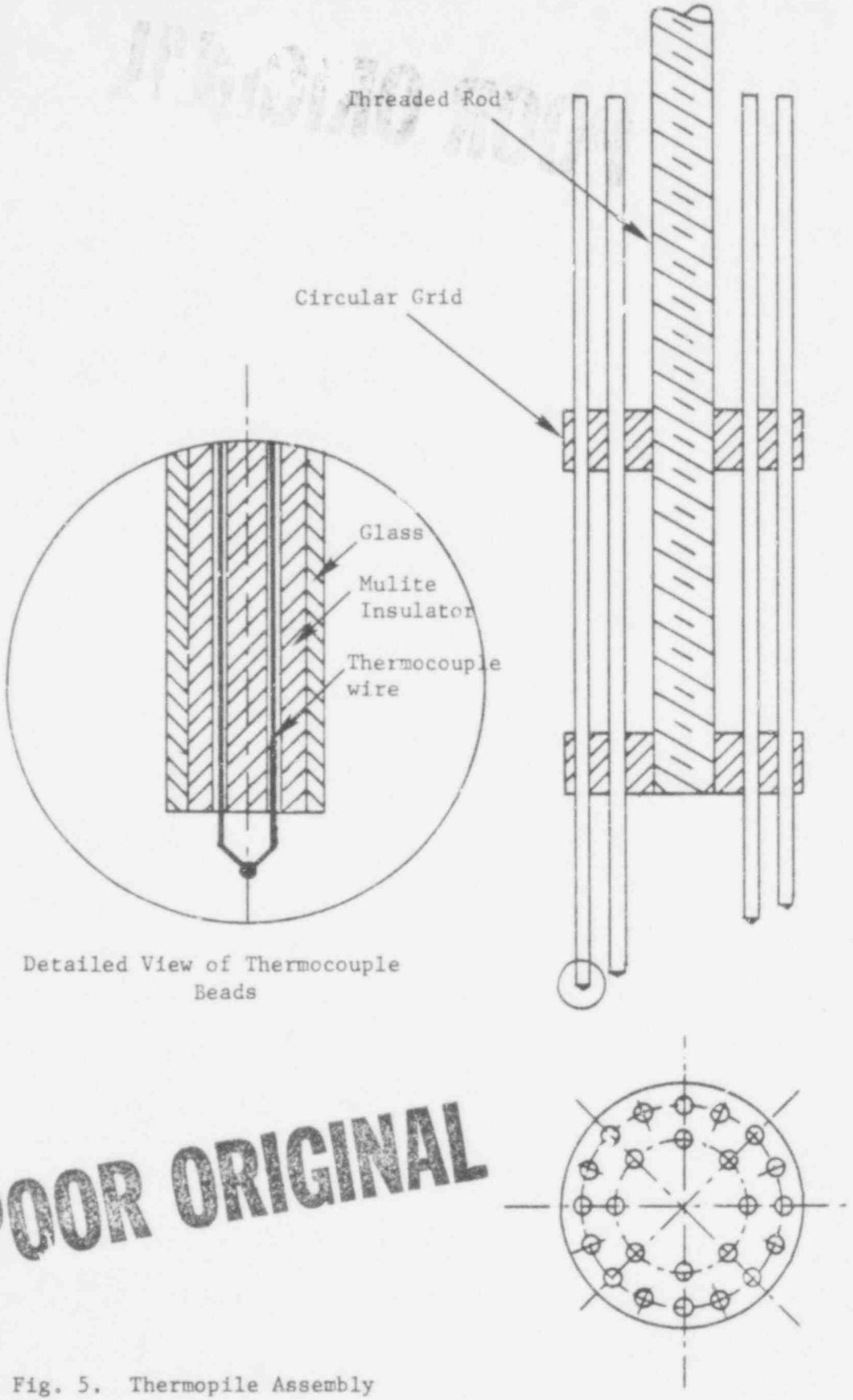

Fig. 5. Thermopile Assembly

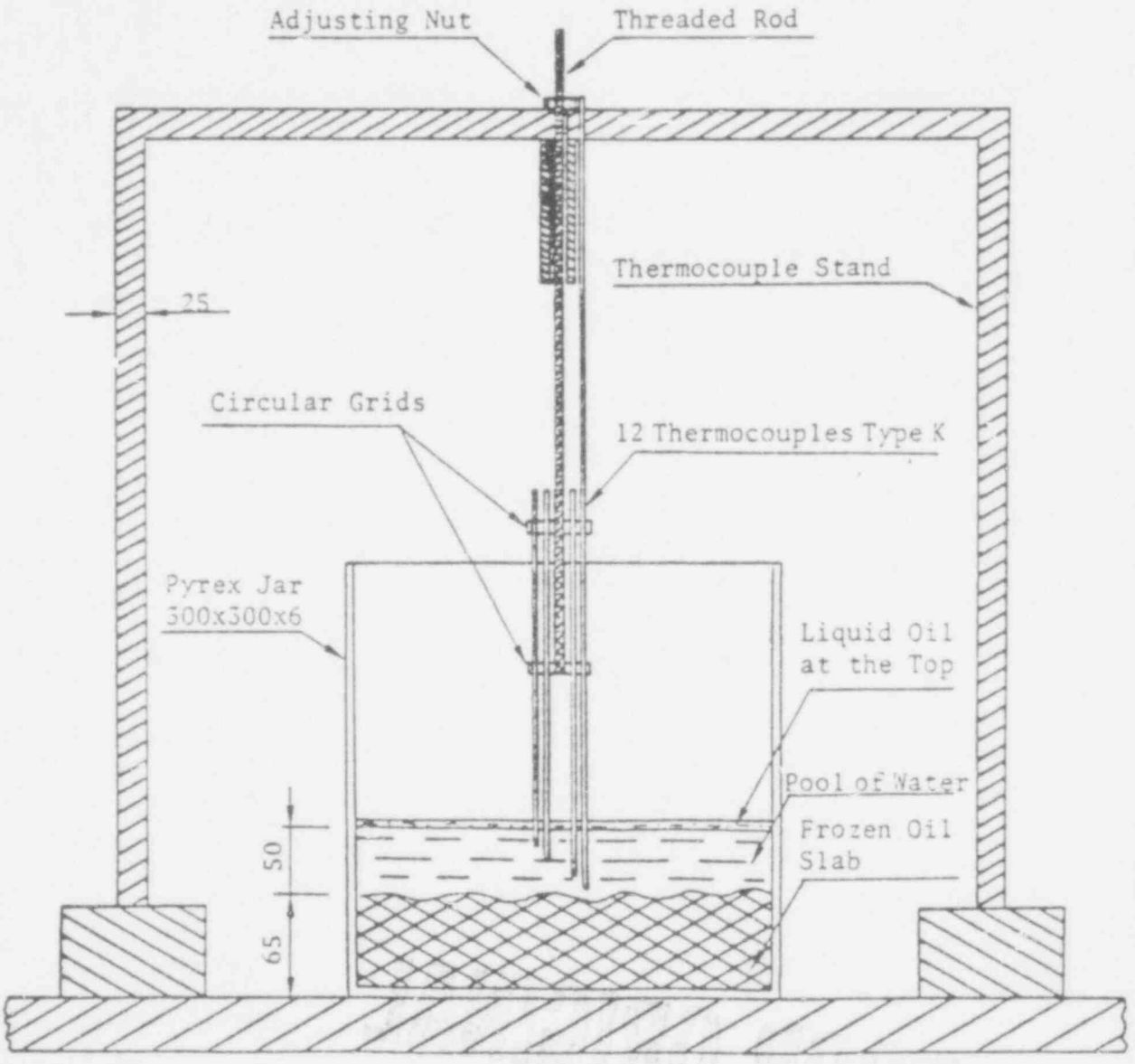

Fig. 6. Test Apparatus.

the interface of the pool and the melt layer and the temperature of the olive oil layer overlaying the free surface of the pool. Two Houston X-Y recorder were used to record the thermopile output and temperature of either olive oil layer or the interface between melt layer and the pool. A selector switch was used to monitor either the olive oil layer temperature or the pool-melt layer interface temperature. The Houston X-Y recorders were equipped with time basis (x-axis) having variable speeds of, 0.1, 0.2, 0.5, 1, 2, 5, 10, 20, and 50 sec/in. The voltage axis (y-axis) could have sensivities of 0.1, 0.2, 0.5, 1, 2, 5, 10, 20, and 50 mv/in. With the recorder used to monitor thermopile output, a Leads and Northrup potentiameter was used to provide a negative offset voltage in case that the output was out of the range of the recorder. The potentiameter could provide voltages varying from 0.01 to 100 mv with an accuracy of 0.01 mv.

2. Experimental Procedure

After freezing approximately a 6.5 cm thick layer of olive oil in the refrigerator, the pyrex jar containing frozen olive oil was placed on a styrofoam sheet and visual observations were made to assure that the surface of the slab was as nearly horizontal as possible and the slab was not cracked. Thereafter the position of the thermopile was adjusted so that the lowest thermocouple would touch the slab surface. About 4 kg of distilled water was heated to the desired temperature. The precise weight of the water was then noted and it was quickly poured into the pyrex jar. Thereafter the x-y recorders were started, and the mean temperature of the pool was recorded as a function of time on one of the recorders. The temperatures of interface and olive oil layer overlaying pool free surface were recorded alternatively

on the second recorder. The data obtained during the first 3 to 5 minutes were ignored because of the following two reasons:

(i) Strong transient effects due to heat absorbed by the cold pyrex jar were present during this time.

(ii) During this time, enough olive oil would have been melted to form a thin layer overlaying the pool free surface. The presence of the olive oil layer would significantly reduce the heat loss due to evaporation from the pool free surface.

The experiments were repeated with different pool temperatures. The visual observations showed that immediately after the pool of water was formed over the frozen olive oil slab, a thin film of liquid oil was formed between the solid surface and the pool. From this film, liquid droplets were released cyclically. Due to melting, the frozen oil surface tended to recede with time from the fixed location of thermocouples in the thermopile. Thus after an interval of about 2 minutes, the thermopile was moved downward by rotating the nut so that the lowest thermocouple would be at about oil-water interface again. A typical temperature-time plot of thermopile output is shown in Figure 7. At point A, after the location of lowest thermocouple was fixed at the oil-water interface, data recording was started. After about 2 minutes, when the thermopile output corresponds to point B in Figure 7, the thermopile location was adjusted such that the lowest thermocouple was again at the oil-water interface. Actual pool mean thermocouple plot would have been line AC, had one been moving the thermopile at the same rate as the melting surface would recede. Thus, to calculate the total enthalpy loss of the pool per unit area of the slab,

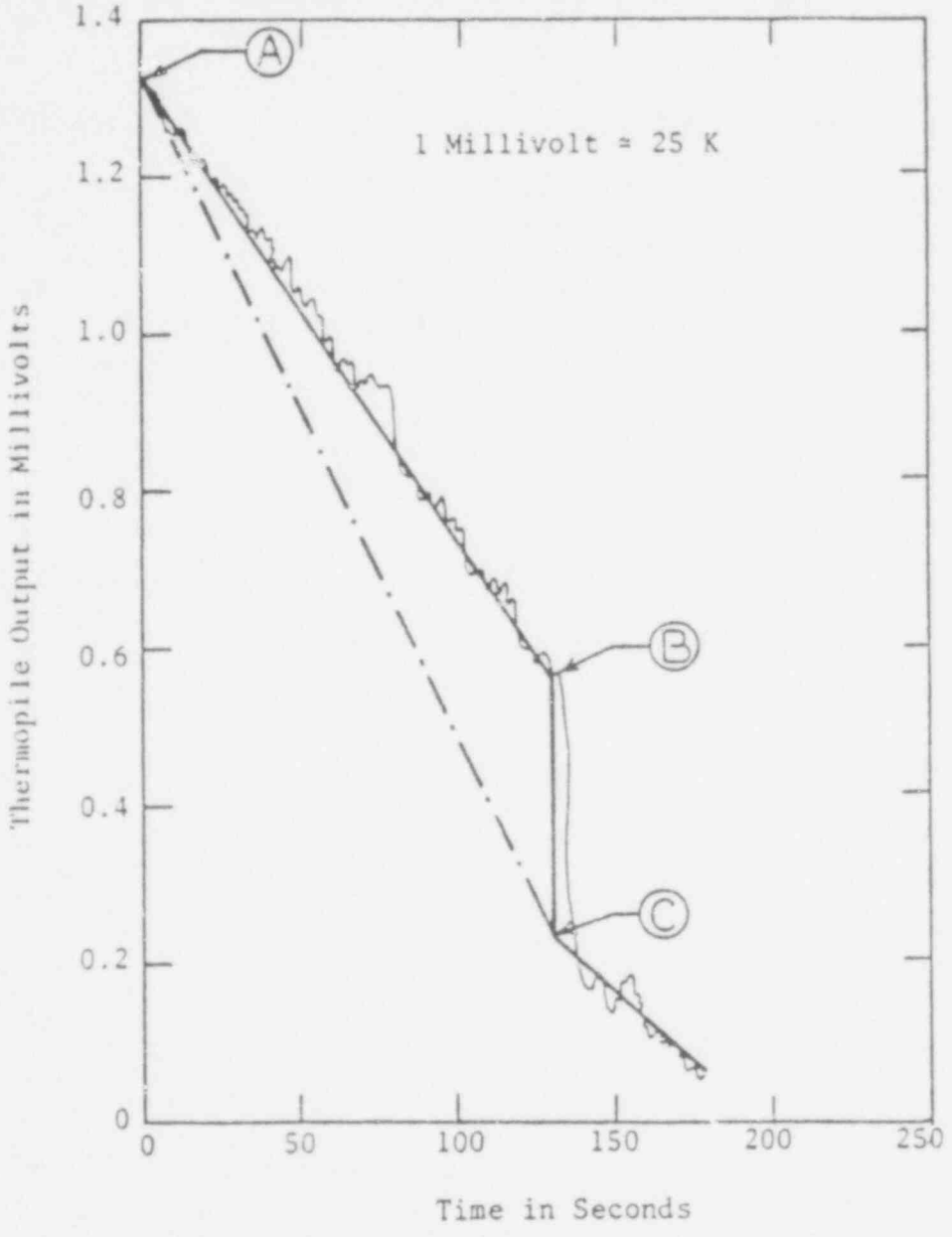

Fig. 7. Typical Temperature Output of the Thermopile.

q_r, the slope of line AC was multiplied by the mass of water in the pool and specific heat of water and divided by products of the area of the slab and the number of thermocouples (ten). The error in obtaining raw heat flux is calculated in Appendix B and is found to be less than $\pm 6\%$.

To obtain the net heat flux q, across the melt layer when the slab is at melting temperature, heat losses are to be subtracted from the observed raw heat flux, q_r. The following mechanism contributed to the losses not accounted for in the theoretical model.

(a) Heat loss to surrounding, q_ℓ: This heat loss was calculated by noting the loss of enthalpy of the pool when the slab of frozen olive oil was replaced by a disc of insulating material (bakelite) of the same thickness as the olive oil slab. In these experiments the pyrex jar was placed in the same refrigerator for sufficient time so that would be chilled to the same temperatures as in actual experiments. Then the chilled pyrex jar was placed on the styrofoam sheet. The position of thermopile was adjusted like in actual experiments and then the pool of warm water was formed over the insulating material. The x-y recorder was started and the mean pool temperature as a function of time was recorded. To have the experimental conditions in the heat loss experiment even closer to the real one, a thin layer of olive oil was formed at the pool free surface. The heat loss experiment was repeated for different initial pool temperatures. Figure 8 shows the plot of the heat loss as a function of the mean pool temperature for three different

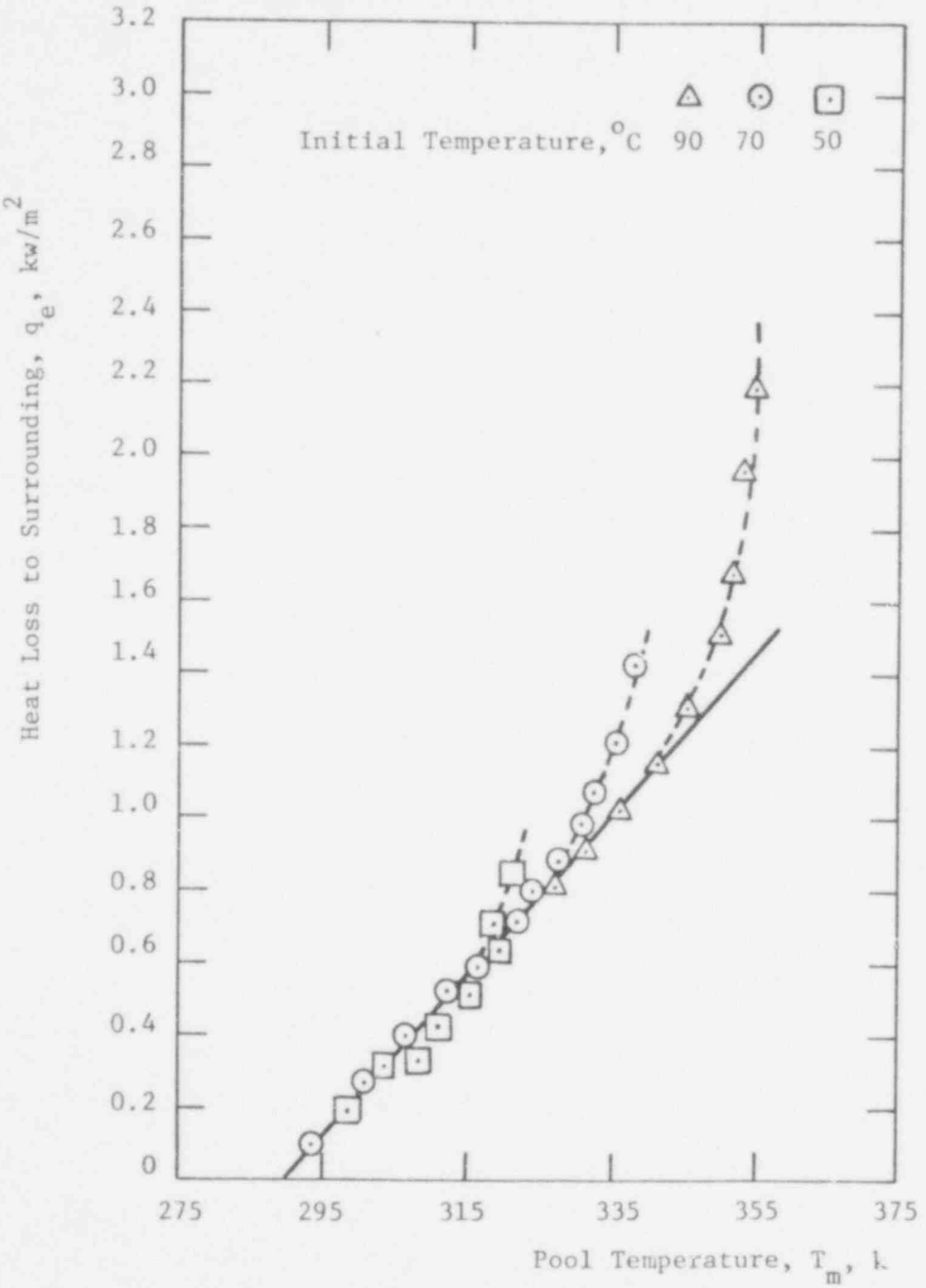

Fig. 8. Heat Loss to Surroundings as a Function of Pool Mean Temperature

initial temperatures. It is observed that transient effect tended to disappear for data taken after about 5 minutes. For times greater than about five minutes, the heat loss was found to be independent of initial temperature of the pool and was only dependent on pool mean temperature. The overall error in calculating the heat loss to the surroundings is found in Appendix B to be less than ± 3%.

(b) Heat loss by conduction to the subcooled slab, q_c: Not all the heat transfer across the melt layer is accounted for in predictions, but small amount of heat is lost from the melting surface by conduction to the subcooled slab. After the pool of warm water has been formed over the subcooled slab a thin layer of melt cover the slab surface. This surface would suddenly be subjected to its melting temperature. For all of the data obtained in this work, it was observed that the melting rate was small enough such that the heat could diffuse into the slab faster than the receding rate of the melting surface. The thermal penetration distance, however, was found to be much smaller than the slab thickness during the times of interests. Thus, this heat loss was calculated by using transient heat conduction equation in a semi-infinite slab:

$$q_c = \frac{2k_o (T_s - T_\infty)}{\sqrt{\pi\alpha}\,(\sqrt{t_2}+\sqrt{t_1})} \qquad (19)$$

where T_∞ is the temperature of the subcooled slab and t_1

and t_2 are the times of the initiation of taking data and the termination of the date recording respectively. The error in q_c should be less than ±15%.

(c) Sensible heat loss to olive oil, q_{se}: Additional sensible heat, apart from that to the melt layer, was supplied to olive oil droplets while growing into the pool, escaping through the pool, and when overlaying the pool free surface in the form of a thin layer. This heat loss is calculated by knowing the mass flux of the melt and the temperature difference between the overlaying layer of olive oil and mean temperature of the film. To obtain the mass flux of olive oil a simple model shown in Figure 9 is used. An

$$q_r - q_\ell - q_{se} + \overset{o}{m}'' c_p T_i = \overset{o}{m}''(h_{sf} + c_p \frac{T_i+T_s}{2}) + q_c$$

or

$$q_r - q_\ell - q_{se} - q_c = \overset{o}{m}'' h_{sf}(1 + c_p \Delta T/2h_{sf})$$

using modified latent heat of fusion yields:

$$\overset{o}{m}'' = q/h'_{sf} \tag{20}$$

where q is the net heat flux utilized in melting of olive oil and heating the melt layer up to a mean temperature of $(T_i + T_s)/2$. Using equation (20), one can write the sensible heat supplied to olive oil as:

$$q_{se} = \frac{q}{h'_{sf}} C_{po} \left(T_o - \frac{T_i+T_s}{2}\right) \tag{21}$$

The net heat flux to the film can be written as:

$$q = q_r - q_\ell - q_c - q_{se}$$

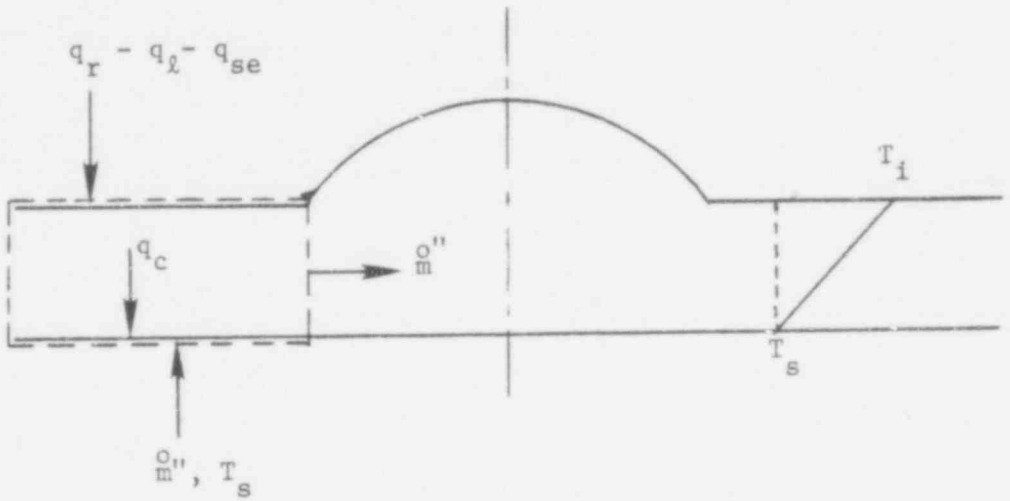

Fig. 9 Physical Model of a Droplet

Equations (21) and (22) were solved simultaneously. The raw and the connected heat flux data are listed in Table 1. Overall maximum error in the neat heat flux, q, is expected to be less than ±8%.

To ascertain the melting temperature of olive oil, a small beaker containing olive oil was placed in the refrigerator. After the oil was frozen, the jar was exposed to ambient laboratory atmosphere for a few hours, then the temperature of the interface of melt oil and frozen oil was measured, and taken as the olive oil melting temperature. This experiment was repeated a few times. The melting temperature was found to be 271.5 K; which is about the value separated in the literature. Tabulated values of viscosity and surface tension for all the temperatures of interest could not be found in the literature. Olive oil viscosity at different temperatures was obtained from extrapolation of available data [14, 15, 16, 17], the temperature correction to surface tenseion was made analytically. The heat transfer coefficient depends weakly on surface tension ($\sigma^{-1/8}$), it may be pointed out that the numerical constant, C in the expression for heat transfer coefficient, equation (17), does not strongly depend on surface tension, since all the derivations have been made using dimensionless parameters. Thus a few percent error in surface tension would contribute to insignificant amount of error in calculation of heat transfer coefficient from equation (17). Complete details of evaluation of viscosity and surface tension are given in Appendix A.

To be able to study the droplet spacing, geometry and growth very carefully, several motion pictures of the experiments have been taken. These movies have been used to reduce the data for the droplet geometry at different stages of growth.

Table 1. Data for Heat Transfer from Water to Olive Oil

Interface Temperature T_i,K	Mean Pool Temperature T_m,K	Temperature of Liquid Oil at the Top T_o,K	Raw Heat Flux q_r,w/m^2	Heat Loss to Surrounding q_ℓ,w/m^2	Total Heat Flux to Oil q_t,w/m^2	Sensible Heat Transferred to Oil q_{se},w/m^2	Conduction to Slab q_c,w/m^2	Corrected Heat Flux q,w/m^2	Heat Transfer Coefficient h,w/m^{2}K
313.6	335.9	328.7	4722	1020	3702	1399	132	2171	52
310.9	332.7	328.6	4346	950	3396	1337	98	1961	50
309.9	343.4	339.0	5358	1200	4158	1915	93	2150	56
305.0	338.5	339.0	4848	1080	3768	1828	75	1865	56
299.1	327.1	328.2	3793	810	2983	1361	73	1549	56
296.4	321.5	318.3	3616	720	2896	1174	100	1622	66
294.0	317.4	313.4	2792	620	2172	831	86	1255	56
287.5	304.7	302.2	1416	150	1266	412	73	781	49
285.6	294.6	294.5	1095	140	955	236	96	623	45
282.9	292.4	294.0	821	120	701	188	58	455	40
282.4	291.5	294.2	698	110	583	160	53	375	35
282.3	290.1	294.2	516	80	436	118	41	277	26
282.1	287.9	293.5	343	45	298	78	31	189	18
281.9	287.0	293.0	284	30	254	65	29	160	16
281.0	285.5	290.7	203	10	193	446	21	126	14
277.5	283.0	--	132	0	132	0	66	66	11
277.3	282.2	--	51	0	51	0	18	33	6

IV. RESULTS AND DISCUSSION

Upon the formation of a pool of warm water over a slab of frozen olive oil, a layer of melted oil was found to separate the surface of the slab from the pool of water. From this layer, oil droplets were observed to regularly be released. The spacing of these droplets was also found to remain constant with time. When the experiments were repeated with water pools of different temeratures, the droplet spacing and size were found to be unaffected, while the droplet release frequency increased significantly with the pool temperature.

Little agitation of the pool of water was observed to occur as a result of the movement of the oil droplets through the pool. Thus, conduction was found to be the dominant mechanism for the transfer of heat from the pool to the olive oil slab. The cooling of the pool at its bottom tended to stratify the pool with time. Therefore, the temperature of the pool varied both with time and with vertical location. Figure 10 shows the variation of the maximum and mean pool temperatures and of the temperature of the interface between the melt layer and water pool with time for a typical experiment. It can be seen that after 4 to 5 minutes the temperature at the top of the pool reached a quasi-static state; as a result, the ratio of the maximum or mean pool temperature to the interface temperature remained nearly constant with time. The temperature gradient of the pool in the vertical direction for one of the quasi-static states is shown in Figure 11. The temperature of the pool reached its maximum near the middle of the pool; thereafter it remained almost constant, before dropping off slightly near the free surface. A slight decrease in water temperature near the free surface was caused by a loss of heat

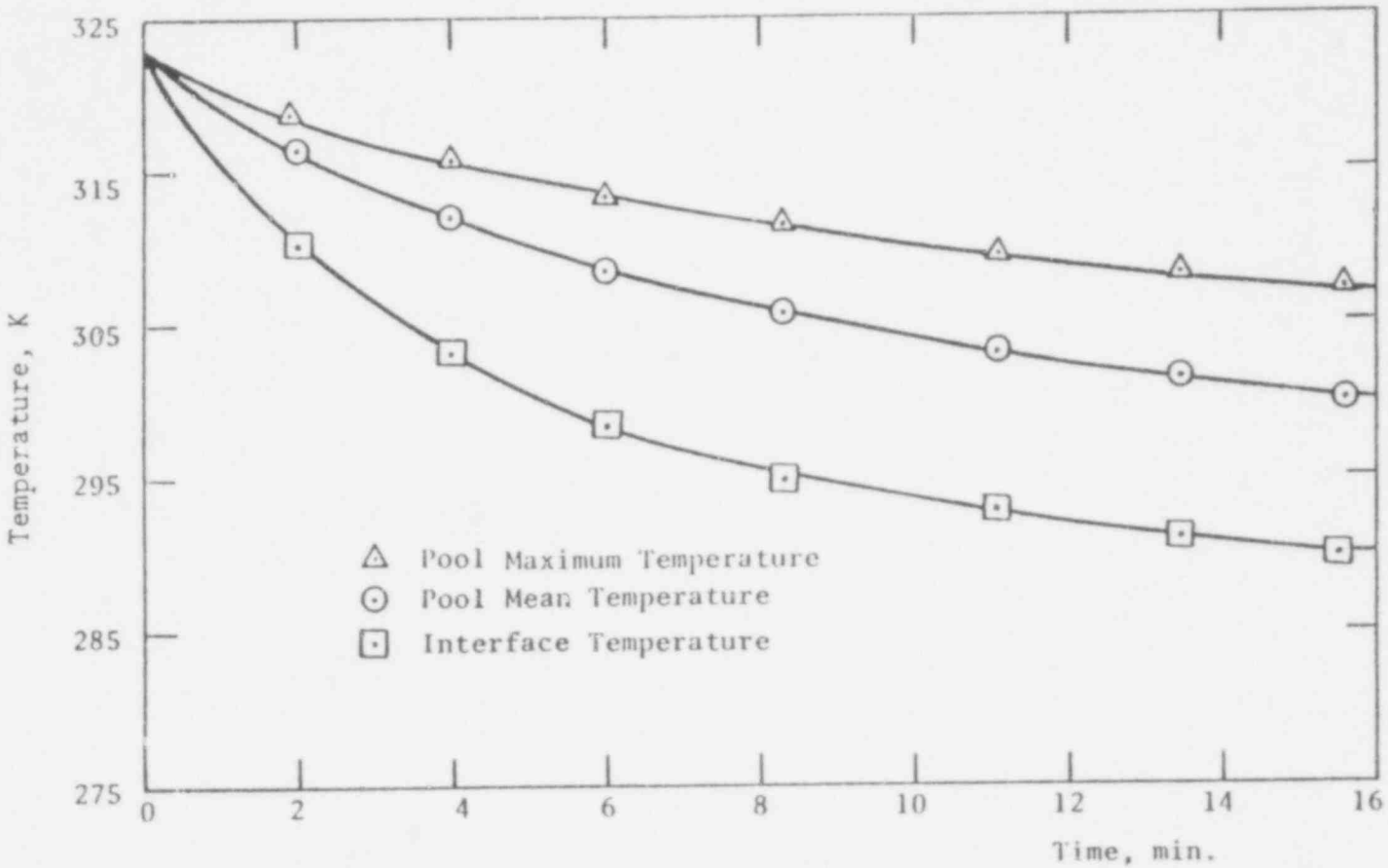

Fig. 10. Pool Maximum, Pool Mean, and Interface Temperature vs Time

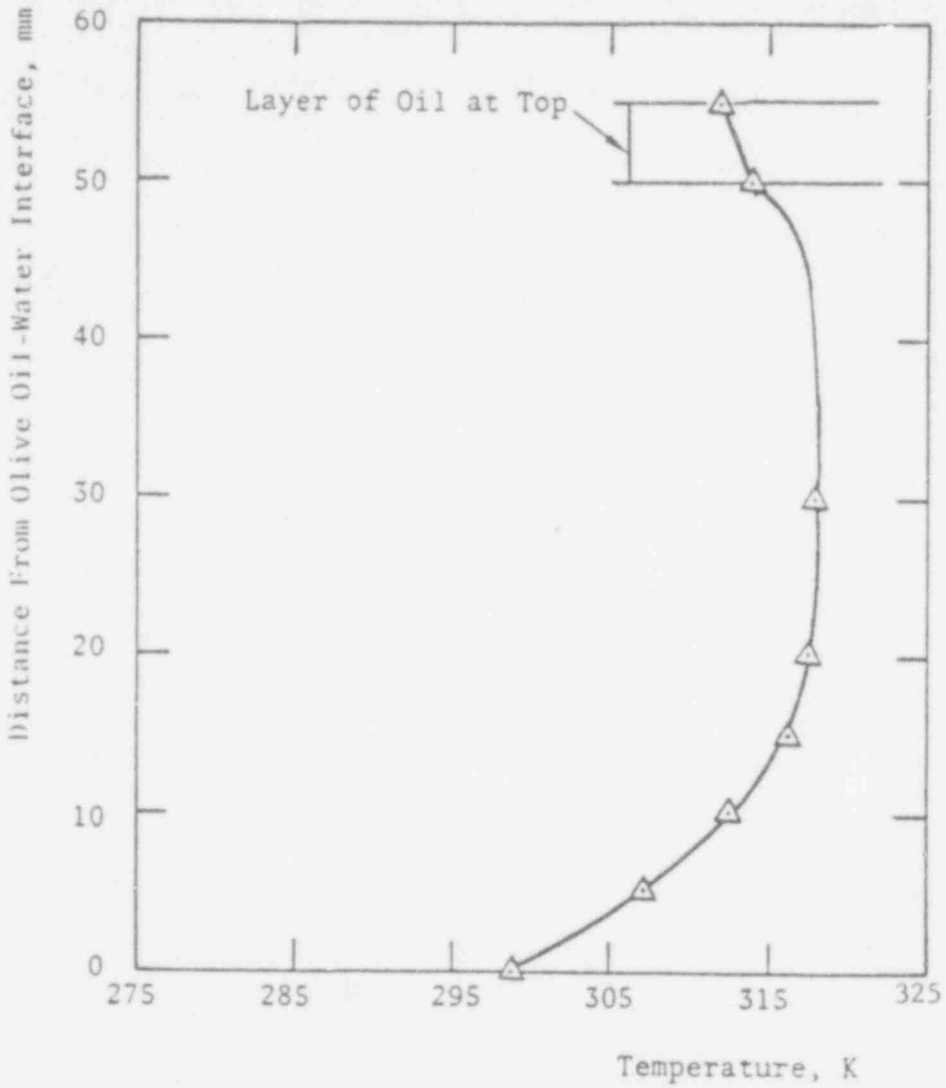

Fig. 11. Temperature of the Pool vs Distance From Interface

to the overylying cooler layer of olive oil. The olive oil layer on top of the pool was generally found to remain cooler than the pool, since it was constantly being fed with cold droplets. Near the interface, the pool temperature decreases nearly linearly and slowly with distance, which confirms the fact that conduction is the dominant mechanism for the transfer of heat from the pool. The quasi-static oil-water interface temperature is plotted in Figure 12 as a function of the mean pool temperature. The interface temperature increases linearly with the mean pool temperature. The few data points marked by circles, and not correlated by the straight line fitting most of the data, correspond to periods soon after the formation of the pool of water over the frozen olive oil slab. During these periods, less than 5 minutes long, transient effects were present.

The photograph in Figure 13a shows a side view of the process of melt removal when a pool of warm water, at a mean temperature of about 323 K, was formed over the frozen olive oil slab. The ridges and valleys on the surface of the slab show a definite wave pattern. The distance between two neighboring droplet-releasing nodes lying over the central part of the slab measures about 5.4 cm. The droplet spacing, and arrangement, are slightly distoreted near the edges of the slab. The first row of droplets seen in Figure 13a lies next to the edge of the slab and has a droplet spacing less than that in the interior of the slab. Figure 13b, which was obtained during preliminary experiments, shows a top view of the frozen oil slab after the pool of water has been drained out. A square pattern and a three-dimensional Taylor wave are clearly visible in this picture. The average spacing between the nodes of droplet release was measured to be between 4.7 and 5.4 cm, (0.75 to 0.85 λ_d), whereas the

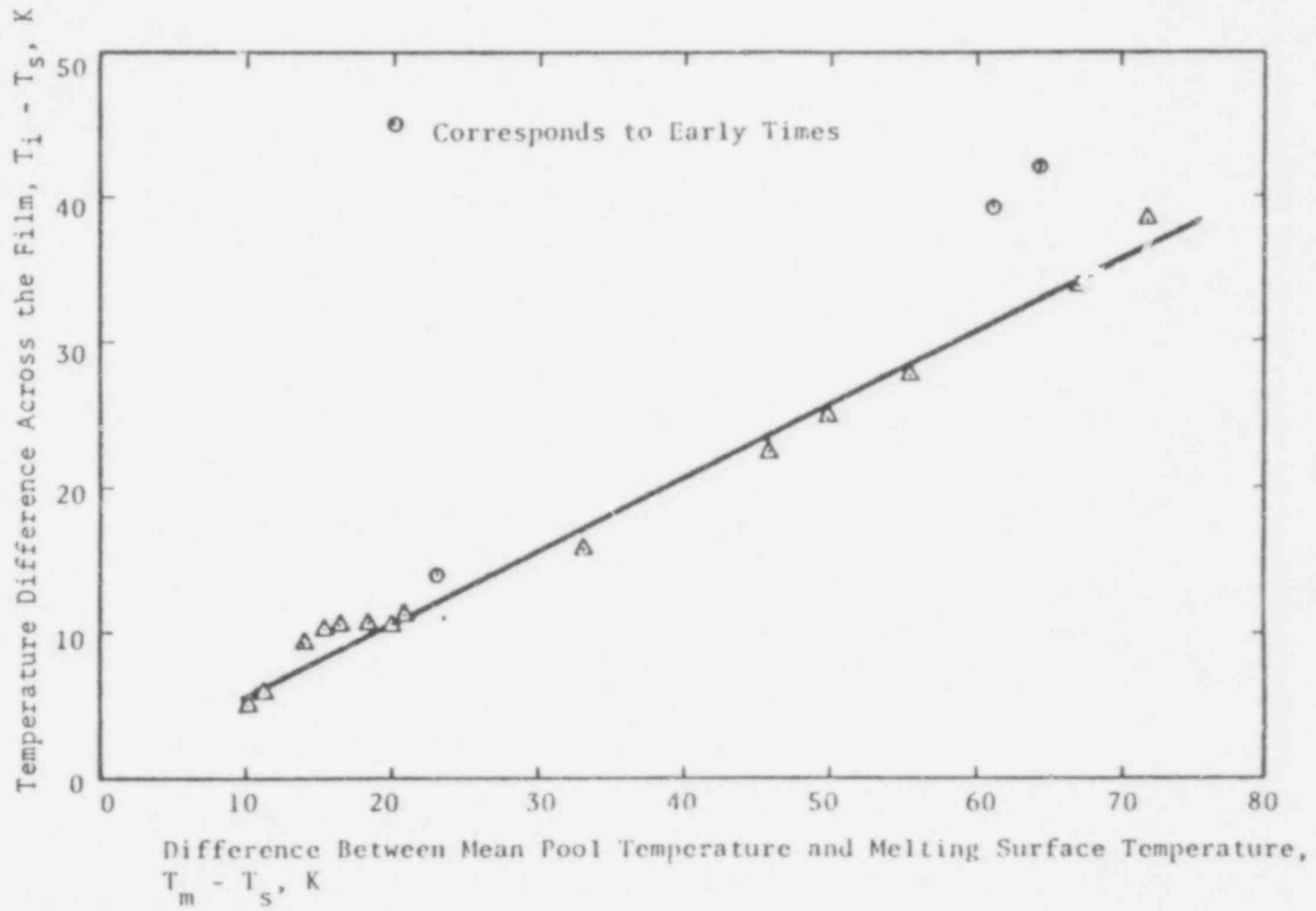

Fig. 12. Relation Between Mean Pool Temperature and Interface Temperature

a. Side View

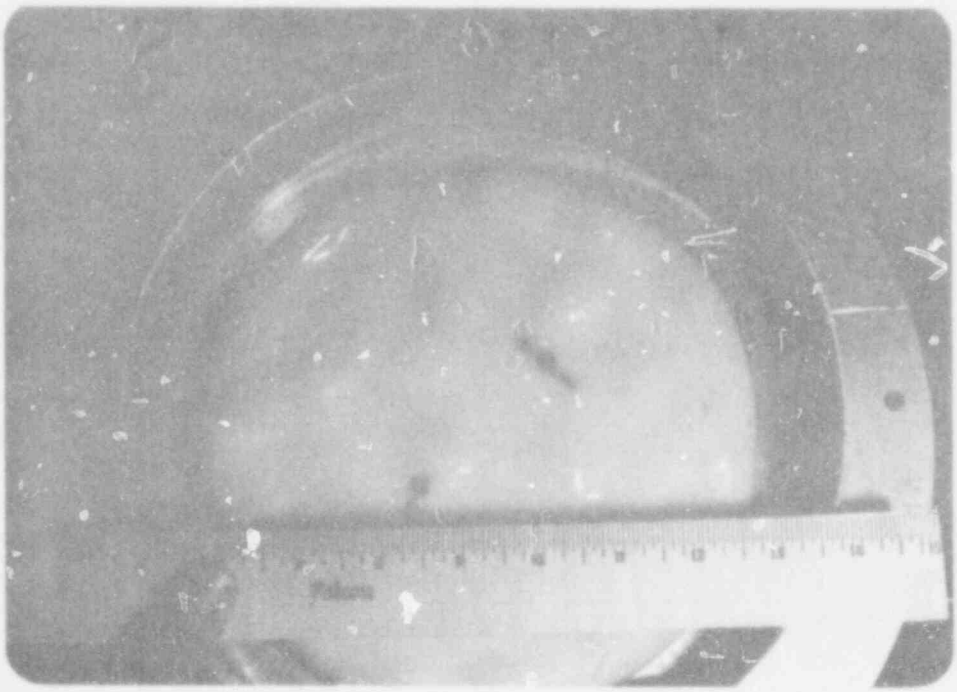

b. Top View

Fig. 13 Photograph of Melting of Olive Oil $\lambda \approx 5.4$ cm (Scale in Picture is in Inches).

two-dimensional "most dangerous" Taylor wavelength, based on linear, viscous, immiscible analysis for fluids of infinite depth, is predicted to be 6.28 cm (see Appendix C). The difference in height between peaks and valley tended to increase as the melting progressed, and was observed to reach a limiting value of about $\lambda/6$.

The dependence of the interface height on the time required for a droplet growth and release cycle has been studied for several droplet releasing sites. A typical interface height as a function of time is plotted in Figure 14. During the first quarter of the cycle, the interface is seen to maintain its near-equilibrium position. Visual observations showed that during this period, the interface tended to smooth out any distortion of itself caused by the pinching-off of the droplets during the droplet release period. After this waiting period, the interface started to grow slowly until the droplet began to break away from it; i.e., at a dimensionless droplet height, η^*, of about 1.5. This is exactly the value that was predicted by the theoretical analysis. During the droplet break-away period, the interface protrudes rapidly until the droplet is pinched off from the interface. If the interface height which corresponds to half of the release cycle is taken as the mean droplet height, then other droplet parameters such as droplet radius, R^*, droplet base radius, r_1^*, and the radius of the equivalent cirlce, r_2^*, at the mean droplet height can be compared with those parameters predicted by the analysis (see Equations (4) and (6)). Table 2 compares the predicted parameters with those obtained from two droplet observations made from the movies. The predictions are in good agreement with the data.

Figure 15 shows the observed amplitude of the olive oil-water interface as a function of time for three different droplets on a log scale.

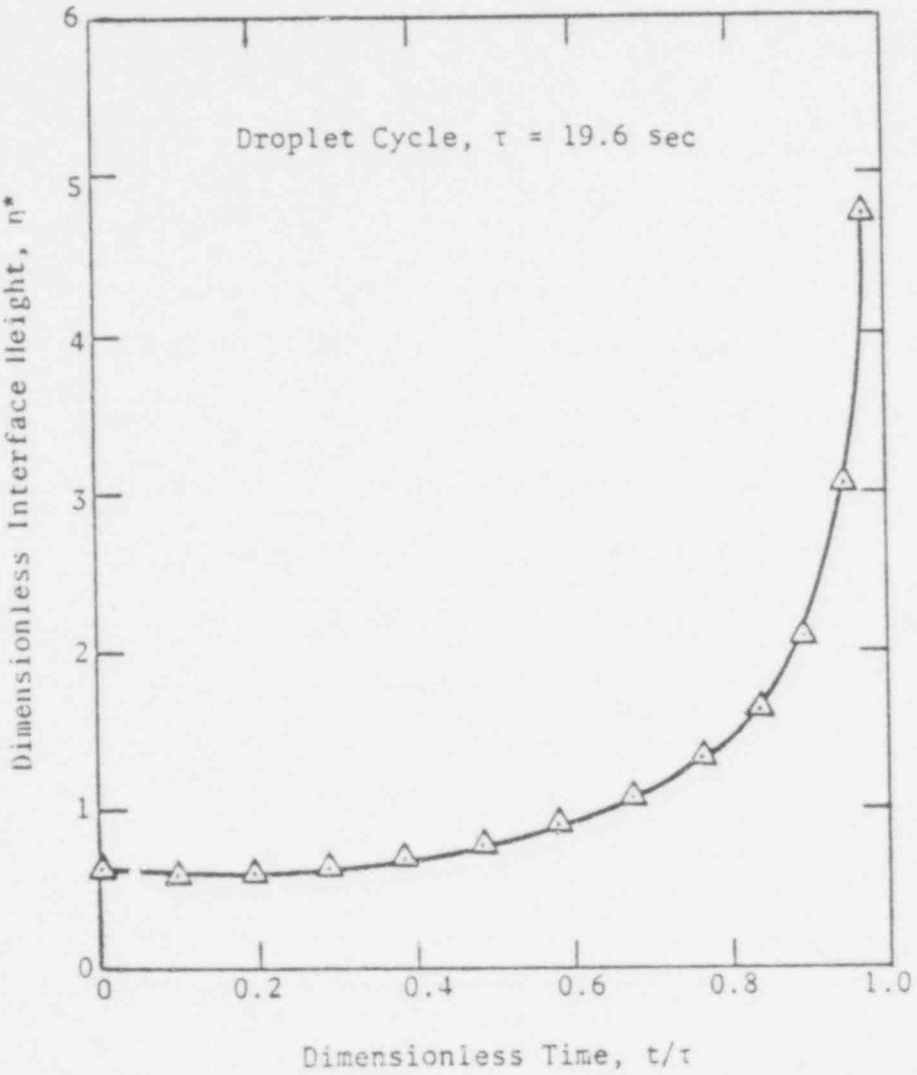

Fig. 14. Interface Height as a Function of Time During One Cycle

Table 2. Comparison of Droplet Data With the Predictions

	Dimensionless Droplet Radius R^*	Dimensionless Droplet Chord Length r_1^*	Dimensionless Cell Radius r_2^*	Mean Interface Height η^*	Constant for Heat Transfer Coefficient C
Data (i)	3.6	2.3	5.7	0.85	0.20
(ii)	4.1	2.2	5.9	0.80	0.20
Predictions Based on $\lambda = 0.8\ \lambda_d$	4.6	2.6	5.6	0.9	0.22

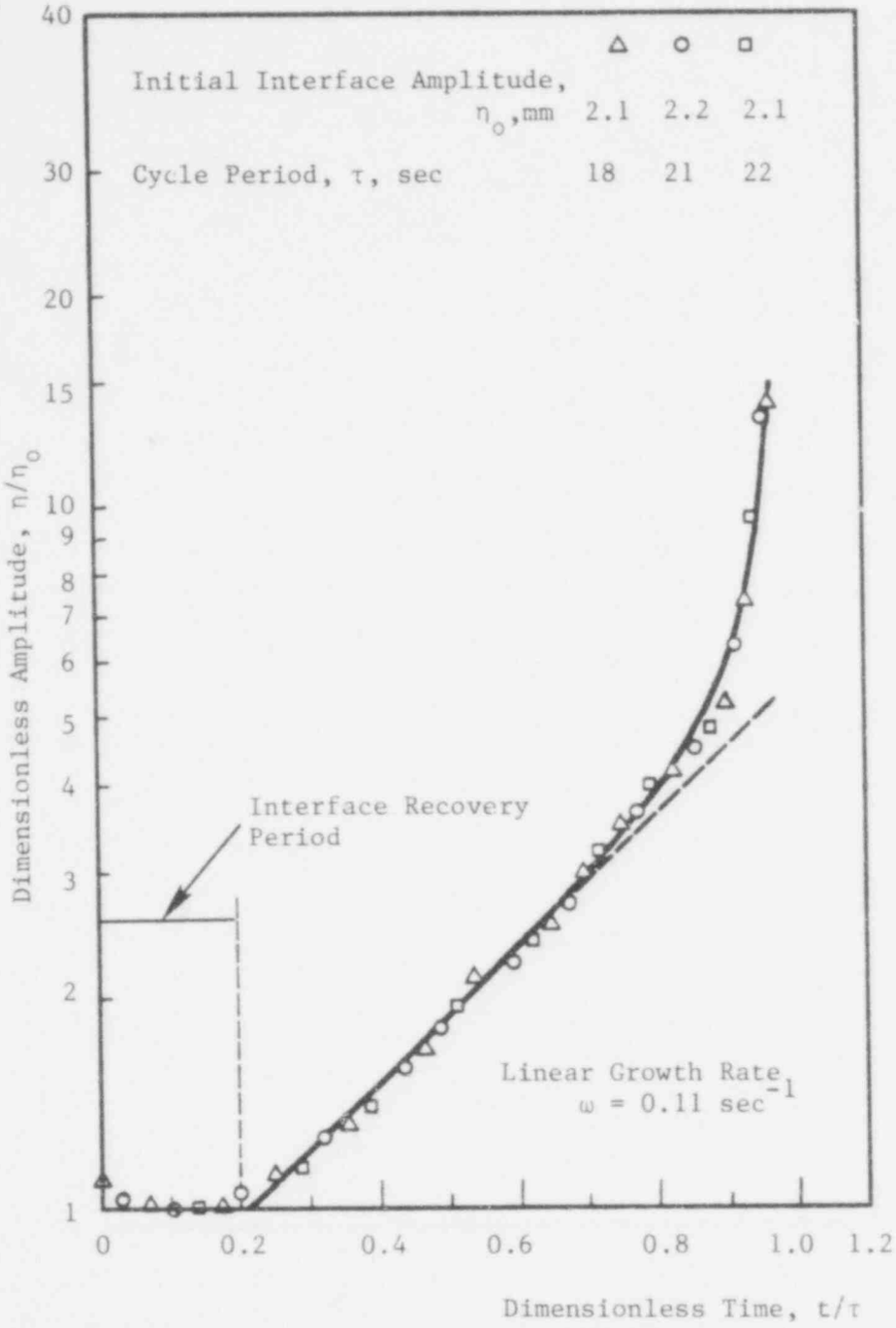

Fig. 15 Dimensionless Interface Amplitude as a Function of Time for One Cycle.

The slope of the linear part of the plot, growth rate, is 0.11 sec^{-1}. The growth rate of the interface predicted by stability theory for viscous liquids of infinite depth is plotted in Figure 16 as a function of the wavelength of the disturbance. The growth rate, ω, starts from 0 for the critical wavelength and increases very rapidly as the wavelength approaches its most dangerous value. The growth rate is greatest for the most dangerous wavelength and thereafter drops slowly as the wavelength becomes large. In this figure the range of wavelengths observed in the present experiments and the growth rate as obtained from Figure 15 are also plotted. Note that the interface growth rate in the experiments is about 50 times slower than would be predicted for the fastest-growing wavelength. This confirms the assumption made in Chapter 2 that equilibrium exists between surface tension and buoyant forces for the present system (small density differences). Furthermore, the observed wavelengths lie between the critical and "most dangerous" ones, and for these wavelengths as seen from Figure 16 a slight change in wavelength results in a large change in growth rate. Therefore, taking into consideration error in measurement, and also the presence of edge effects, it is possible to have a much smaller growth rate than that demanded by the observed wavelengths.

The data for heat transfer across the melt layer when the slab is assumed to be maintained at its melting temperature are plotted in Figure 17 as a function of the difference in temperature between the interface and the slab. The heat flux is observed to increase as $\Delta T^{3/4}$ for temperature differences greater than 20 K, as would be expected from Equation (17). For temperature differences smaller than 20 K, the heat flux starts to drop more rapidly, until ΔT reaches 10 K. At a temperature difference of about 10 K the droplets cease to appear on the slab surface.

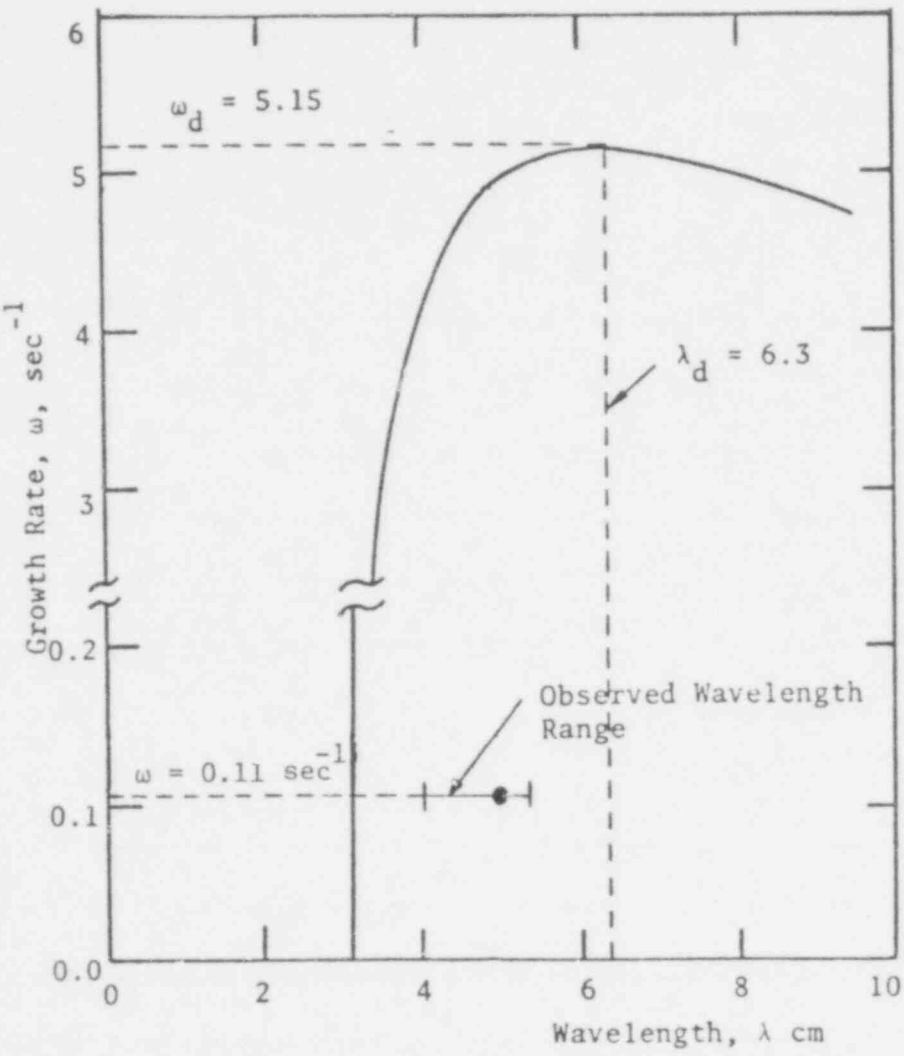

Fig. 16. Comparison of Observed and Predicted Wavelength and Growth Rate

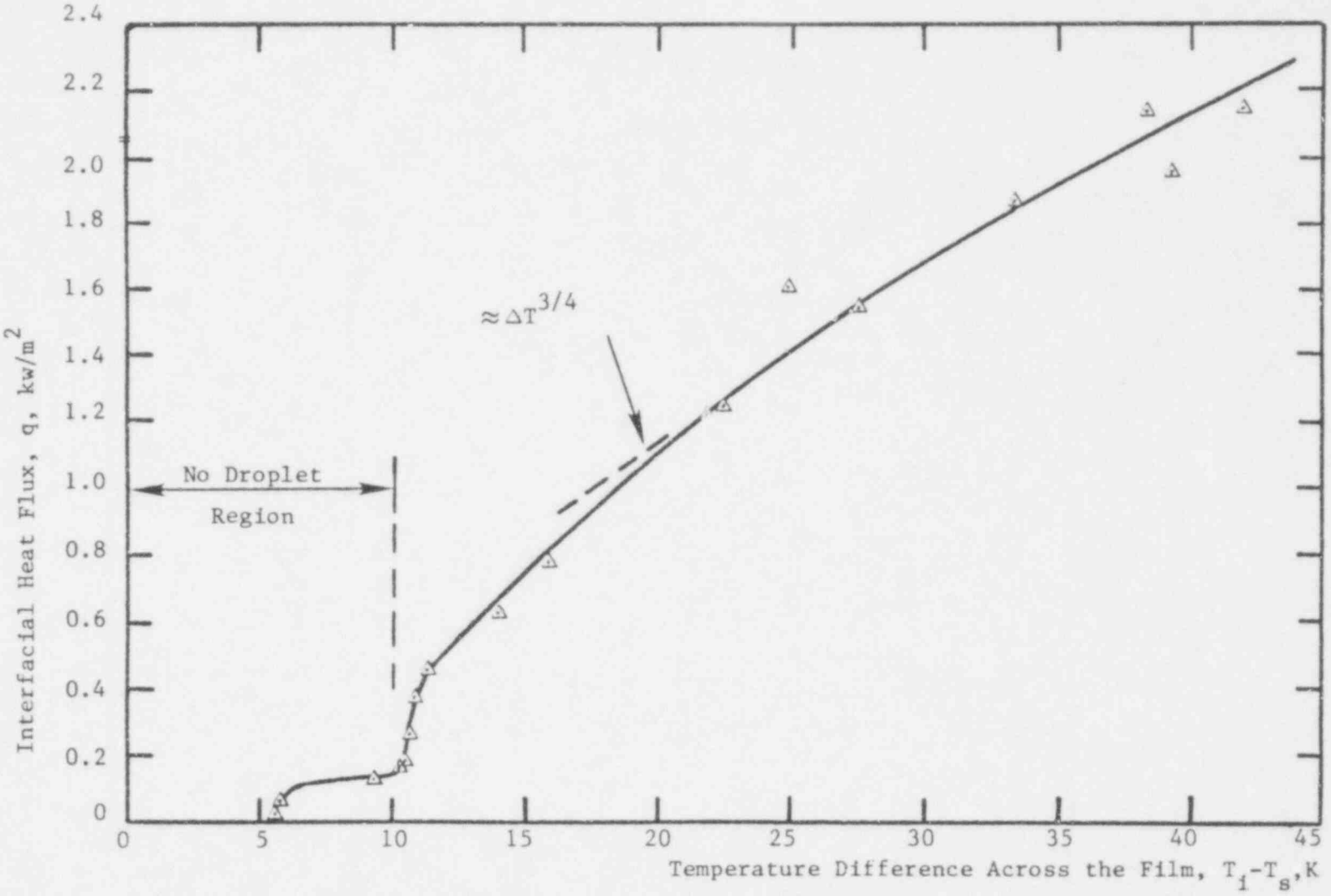

Fig. 17 Dependance of Interfacial Heat Flux on Temperature Difference Across the Film

Now the melted olive oil does not leave the slab surface, and simple conduction is thought to occur between a stagnant layer of melt on the slab surface and the water. This mode of heat transfer occurs until the temperature difference drops to 5.5 K. For ΔT below 10 K the heat flux decreases nearly linearly until it becomes almost 0 at a temperature difference of about 5.5 K. This temperature difference corresponds to an interface temperature of 277 K. Water at 277 K (4°C) is denser than at any other temperature; thus, once the pool temperature reaches 277 K at the interface, it remains at this value until the whole pool reaches the same temperature of 277 K. The experiments, however, were ended long bedore this could happen.

Figure 18 shows the dependence of the heat transfer coefficient on the temperature difference across the film. It can be seen that for temperature differences greater than 20 K, the behavior of the heat transfer coefficient is in good agreement with predictions, while the data are about 20 to 25% lower than predicted. It should be noted that the predictions are based on an estimated value of $\lambda = 0.8\ \lambda_d$ and an average value of η^*. However, if the predictions were based on the observed values of λ and η^* as given in Table 2, the data would only be about 15% lower than the predictions. As the temperature difference becomes less than 20 K, the heat transfer coefficient drops considerably below the predictions. For ΔT less than 20 K, the cyclic release of droplets breaks down and droplets are released at random. For these temperature differences the film model developed earlier does not hold up very well. At a temperature difference of 10 K, the heat transfer coefficient drops quickly and remains almost constant until $\Delta T = 5.5$ K. In this temperature range, as mentioned earlier, the droplets are no longer released.

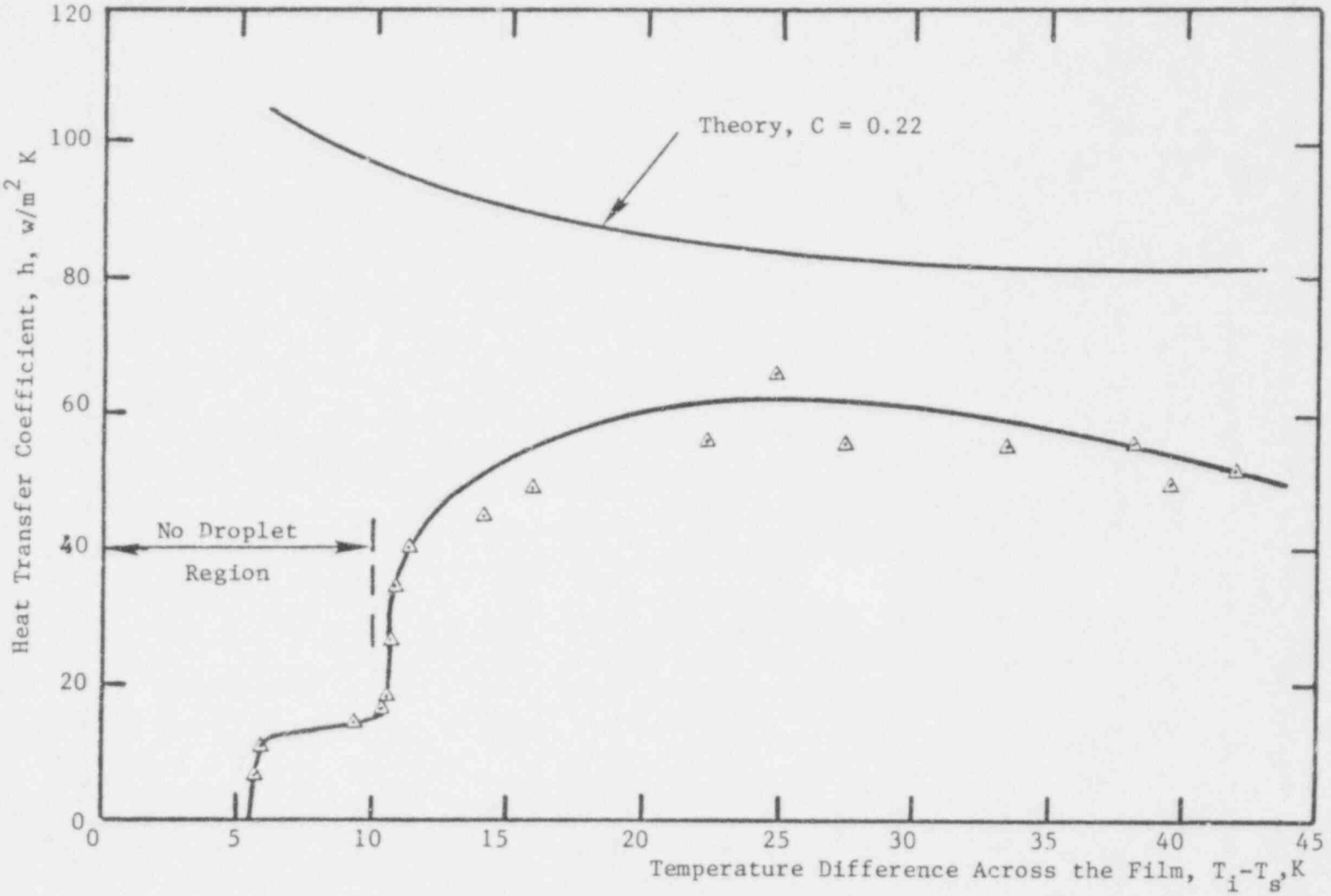

Fig. 18 Dependance of Heat Transfer Coefficient on Temperature Difference Across the Film

In the region of $5.5\ K < \Delta T < 10\ K$, where the heat transfer is dominated by conduction, the heat transfer coefficient is expected to be very small. At a temperature difference of about 5.5 K the heat transfer coefficient suddenly drops almost to 0 . Now the melt layer is constantly exposed to water at 277 K. The small difference in temperature is insufficient to cause enough melting to allow the melt in the film to move and feed the droplets.

Data for the heat transfer coefficient based on the difference between the mean pool temperature and the temperature of the melting surface are plotted in Figure 19. A prediction based on the difference between the mean pool and slab melting temperatures is also plotted. The data are found to be about 60% lower than the predictions. This figure shows that an incorrect heat transfer coefficient may be obtained if stratification of the pool is not considered and the heat transfer coefficients are not based on the melt-water interface temperature.

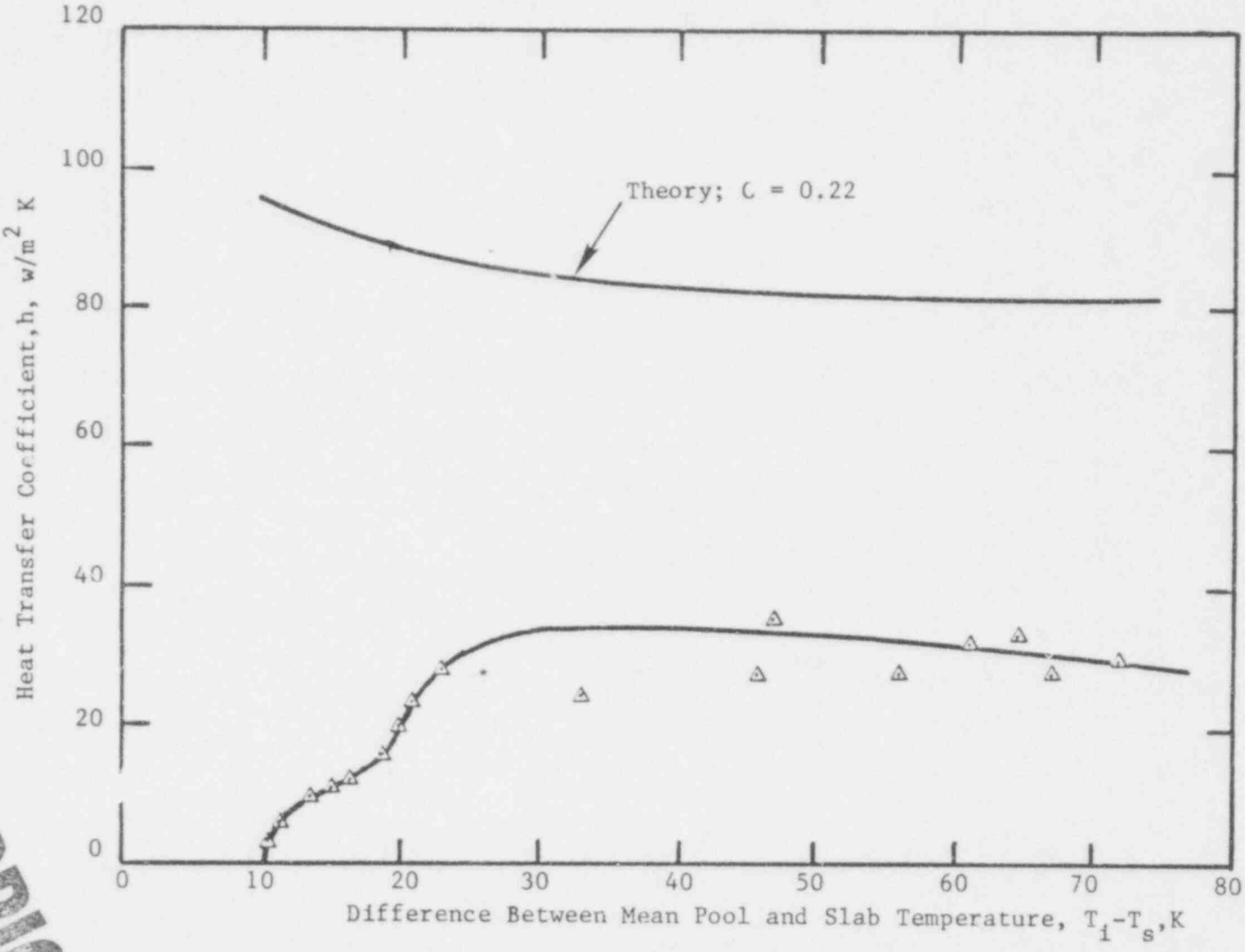

Fig. 19 Dependance of Heat Transfer Coefficient on Mean Pool Temperature.

V. SUMMARY AND CONCLUSIONS

1. Melting of a less dense material placed underneath a heavier liquid has been shown to be governed by Taylor instability.
2. A completely theoretical model based on equilibrium between surface tension and buoyant forces acting on the perturbed interface has been developed to describe the melting process.
3. Data for the droplet radius, droplet base radius, and the droplet height are found to compare favorably with the predictions.
4. Droplet sizes and spacing are not affected by the change of the pool temperature, however droplet frequency was found to be strongly dependent on the pool temperature.
5. Heat transfer coefficient data obtained for interface and melting surface temperature differences greater than 20 K are found to be about 20-25% lower than predictions.
6. Predictions for the heat transfer coefficient should be compared with data based on interface temperature rather than on pool mean temperature.
7. Effect of olive oil viscosity on the "most dangerous" wavelength and its growth rate has been studied and viscosity was found to lengthen the "most dangerous" wavelength by 17% and decrease its growth rate by 11%. Viscosity was found to have no effect on critical wavelength.

REFERENCES

1. Taylor, G.I., "The Instability of Liquid Surfaces When Accelerated in a Direction Perpendicular to Their Planes, Part I," Proceedings Royal Society London, A-201, 1950, p. 192.
2. Bellman, R., Pennington, k.H., "Effects of Surface Tension and Viscosity on Taylor Instability," Quart. Appl. Math., Vol 12, 1954, p. 151.
3. Zuber, N. "Hydrodynamics Aspects of Boiling Heat Transfer," AEC Report No. AECU-4439, Physics and Mathematics, 1959.
4. Berenson, P.J., "Film Boiling Heat Transfer From a Horizontal Surface," JOURNAL OF HEAT TRANSFER, Trans. ASME, Series C, Vol. 83, No. 1, 1961, pp. 351-362.
5. Berenson, P.J., "Experiments on Pool-Boiling Heat Transfer," International Journal of Heat and Mass Transfer, Vol. 5, No. 10, 1962, pp. 985-999.
6. Sernas, V., Lienhard, J.H., and Dhir, V.K., "The Taylor Wave Configuration During Boiling From a Flat Plate," International Journal of Heat and Mass Transfer, Vol. 16, No. 9, 1973.
7. Dhir, V.K., Castle, J.N. and Catton, I., "Role of Taylor Instability on Sublimation of a Horizontal Slab of Dry Ice," Journal of Heat Transfer, Trans. ASME, Vol. 99, No. 3, 1977.
8. Alsmeyer, H. and Reimann, M., "On the Heat and Mass Transport Processes of a Horizontal Melting or Decomposing Layer Under a Molten Pool," paper presented at the Nuclear Reactor Safety Heat Transfer Symposium, Winter Annual ASME meeting, pp. 47-53.

9. Dhir, V.K., Castle, J.N., Catton, I., Kastenberg, W.E., and Doshi, J.B., "Role of Wall Heat Transfer and Other System Variables on Fuel Compaction and Recriticality," Int. Meeting on Fast Reactor Safety and Related Physics, Vol. III, p. 1172.

10. Abadzic, E. and Goldstein, R.J., "Film Boiling and Free Convection Heat Transfer to Carbon Dioxide Near the Critical State," International Journal of Heat and Mass Transfer, Vol. 13, 1970, pp. 1163-1175.

11. Hesse, G., Sparrow, E.M., Goldstein, R.J., "Influence of Pressure on Film Boiling Heat Transfer," Journal of Heat Transfer, Vol. 98, 1976, p. 166.

12. Dhir, V.K., and Lienhard, J.H., "Taylor Stability of Viscous Fluids with Application to Film Boiling," International Journal of Heat and Mass Transfer, Vol. 16, No. ' , Nov. 1973, pp. 2097-2109.

13. Plesset, M.S., and Whipple, C.G., "Viscous Effects in Rayleigh-Taylor Instability," Physics of Fluids, Vol. 17, No. 1, 1974.

14. Hsieh, D.Y., "Effects of Heat and Mass Transfer on Rayleigh-Taylor Instability," Trans. ASME, Journal of Basic Engineering, Vol. 94, No. 1, March 1972, pp. 156-162.

15. International Critical Tables, Volume 2.

16. Eckey, E.W., Vegetable Fats and Oils, Reinhold Publishing Corporation, 1954.

17. Bailey, A.E., Oil and Fat Products, Interscience Publishers.

18. Reid, R.C., Prausnitz, J.M., and Sherwood, T.K., The Properties of Gases and Liquids," McGraw-Hill Book Company.

19. Batchelor, G.K., An Introduction to Fluid Dynamics, Cambridge University Press, 1967.

20. Hartridge, H., and Peters, R.A., "Surface Tension Between Olive Oil-Water," Proc. Physiol., October 16, 1920 J. Physiol. 54 xli.

21. Edwards, D.K., Denny, V.E., Mills, A.F., Transfer Processes, Hemisphere Publishing Corporation, 1976.

APPENDIX A

THERMOPHYSICAL PROPERTIES OF OLIVE OIL

The thermophysical properties of olive oil collected from various sources are listed here. The data on latent heat of fusion of olive oil could not be found in the literature and was thus obtained in the laboratory.

(i) Viscosity, μ : There are a few data available for viscosity of olive oil at different temperatures. Table A-1 shows these data [15, 16, 17 19]. Based on the theory of liquid viscosity, the viscosity of liquids are expected to vary exponentially with temperature [18]. A variety of experimental values confirm this relationship for all fatty oils [16]. The temperature dependence of viscosity, which is known an Andrade correlation, is written as:

$$\mu = Ae^{B/T} \qquad \text{(A-1)}$$

knowing the viscosity at two temperaures, the constants A and B in Equation (A-1) can be evaluated. Viscosity of olive oil at 293.2 K and 323.2 K [16] yields these constants as

$$A = 6.93 \times 10^{-4} \text{ centipoise}, \quad B = 3389 \text{ K} \qquad \text{(A-2)}$$

Equation (A-1) is plotted along with the available data in Figure A-1. It is seen that the data from different references match the correlation well.

(ii) Surface Tension, σ : The only reported data for surface tension between water and olive oil is found in Reference [19] and it is for interface temperature of 293 K. The reported value at this temperature is 20 dyne/cm. Generally, based on the theory of the liquids, the surface tension between liquids and their own vapour is corrolated by [18]:

Table A-1. Available Data for the Viscosity of Olive Oil

Temperature T,K	288.2	293.2	294.3	311.0	311.0	323.2	338.8	372.1	373.2
Viscosity μ,cp	99.1	77	73.8	42.7	37.7	24	15.4	8.3	7.0
Reference	19	16	15	17	15	16	15	17	15

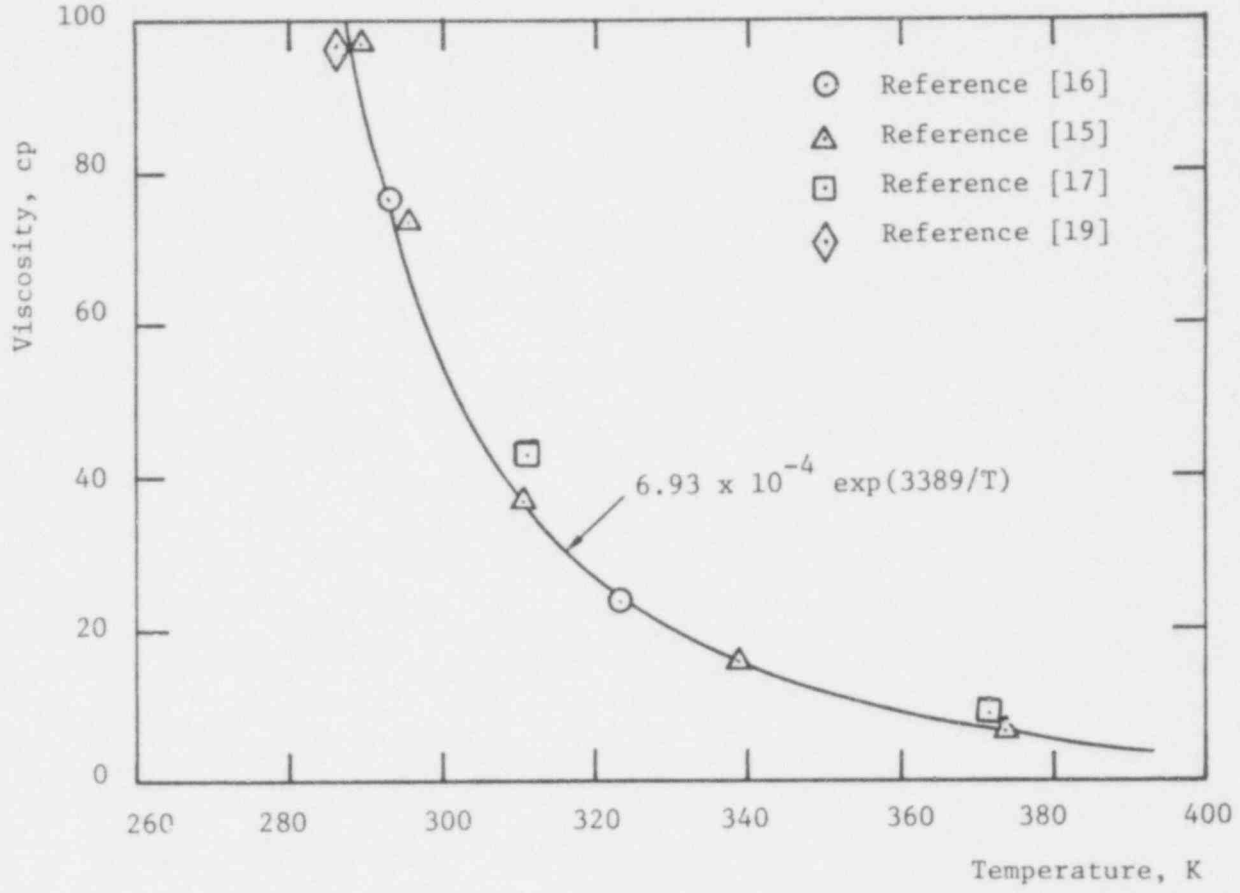

Figure A-1. Dependance of Viscosity of Olive Oil on Temperature

$$\sigma \alpha (1 - T_r)^{4n} \qquad n = 0.25 - 0.31 \qquad (A-3)$$

where T_r is the reduced temperature and n is the empirical constant varying between 0.25 and 0.31. For two immiscible liquids of high and comparable critical temperatures, Equation (A-3) would indicate a very weak dependence of the surface tension on temperature. From this, one could conclude that surface tension between olive oil and water would not significantly depend on temperature. In 1920, Hartridge and Peters [20] reported, "Temperatures between 293 K and 313 K were found to have little effect upon the interfacial tension at water olive oil interface." Therefore, in the present work, it is assumed that in the temperature range of interest (283 K to 303 K) the surface tension between oil and water is not significantly affected by temperature.

(iii) Latent Heat of Fusion, h_{sf} : No data is available for latent heat of fusion for olive oil. Experiments have been conducted by freezing about 250 gm of olive oil in a vacuum bottle. Water has been heated to temperatures about 10 K above ambient, then temperatures of both frozen oil and warm water was noted and water was formed on the frozen oil. After thermal equilibrium the temperature of the mixture was noted and, neglecting heat losses, one could get latent heat of fusion of olive oil by employing conservation of energy. The experiment was repeated a few times and the average latent heat of fusion was calculated about 70 joule/gm.

(iv) Thermal conductivity, k : There are only two pieces of thermal conductivity data available in literature. Thermal conductivity of olive oil at 293 K is reported in reference [19] to be 0.00169 w/cm K while

Reference [15] gives thermal conductivity at 277 K to be 0.00175 w/cm K. However, no data are available for thermal conductivity of frozen olive oil. Comparing olive oil with a few other similar liquids, a value of 0.00145 w/cm K ± 5% is guessed for thermal conductivity of frozen olive oil.

(v) Specific Heat, c_p : Table A-2 shows the available data for specific heat of liquid olive oil. The data listed in Table A-2 shows a reasonable consistency; therefore a mean value of 2.00 joule/gm K is chosen for the temperature range of interest in the present study. No data were found for the specific heat of frozen olive oil, thus a value of 1.70 joule/gm K ± 5% is guessed for specific heat of frozen olive oil near its freezing temperature.

(vi) Density, ρ : The density of liquid and frozen olive oil was obtained both from literature (liquid only) [15, 16, 17, 19, and 21] and from experiments conducted in the laboratory. No significant difference in density of olive oil was observed upon freezing. The value of 0.916 gm/cm^3 is considered for the density of both liquid and frozen olive oil.

Table A-3 shows all the selected values of the different properties of olive oil used in the present work.

Table A-2. Data for Specific Heat of Olive Oil

Temperature, K	----	----	280	293-303	288
Specific Heat $\frac{\text{joule}}{\text{gm K}}$	1.98	2.07	1.97	1.99	2.01
Reference	15	16	17	17	19

Table A-3. Used Values for Properties of Liquid and Frozen Olive Oil

Olive Oil	Viscosity μ, centipose	Surface Tension Between Oil & Water σ	Latent Heat of Fusion h_{sf}, joule/gm	Thermal Conductivity w/cm K	Specific Heat c_p, joule/gm K	Density ρ, gm/cm^3
Liquid	99 (288 K)	20 (293 K)	70	0.00169(288 K)	2.00	.916
Frozen	---	---	---	0.00145 ±5%	1.7 ±5%	.916 ±1%

APPENDIX B

ERROR ANALYSIS

Generally two kinds of errors, systematic and random, exist in an experimental work. Systematic errors are those caused by inadequacies of the equipment, or of the experimentor. Random errors arise because measured values of physical quantities are always associated with mean values of variables subject to fluctuations.

1. Systematic Errors: There are three possible systematic errors in the present experiment, namely, error in the reference temperature, error in the calibration of the recorders and potentiameter, and error in the mass of the pool due to evaporation from the pool free surface. The error due to the reference junction is actually negligible, since it was kept clean and placed in a mixture of ice and water and was checked prior to each experiment. Error in the calibration was also found to be negligible as the recorders and potentiometer were checked periodically. The error due to evaporation is also expected to be negligible, though; it is preferred to show it numerically. Evaporation from a free surface has been discussed in Reference [21]. To evaluate the maximum error we consider the pool to be at 358 K which is the maximum pool temperature at which the experiments were conducted. The ambient air is taken to be at 295 K with a relative humdity of 50%. The physical model used to solve this problem is shown in Figure B-1. To find the convective mass transfer at s-plane one has to know the driving force, namely, density difference between planes s and e. To find the density of a mixture of air and water, ideal gas law and Dalton's law are used;

$$\rho = P_1 M_1/RT + (P - P_1)M_2/RT \ .$$

Symbols used in the analysis for mass loss due to evaporation.

$\mathcal{D}_{12}$	binary diffusion coefficient
g	gravitational acceleration
Gr_L	Grashof number $g\Delta\rho L^3/\rho\nu^2$
j	mass diffusion flow
L	diameter of the jar
M	molecular weight
m_i	mass fraction of species i, ρ_i/ρ
Nu_L	mass transfer Nusselt number, $j_i L/\rho\mathcal{D}_{12}\, m_1$
ν	kinematic voscosity
P	pressure
R	gas constant, 8.3143×10^7 erg/gm-mole K
Sc	Schmidt number, $\nu/\mathcal{D}_{12}$
T	temperature

Subscripts

1	water
2	air
e	ambient
s	saturated

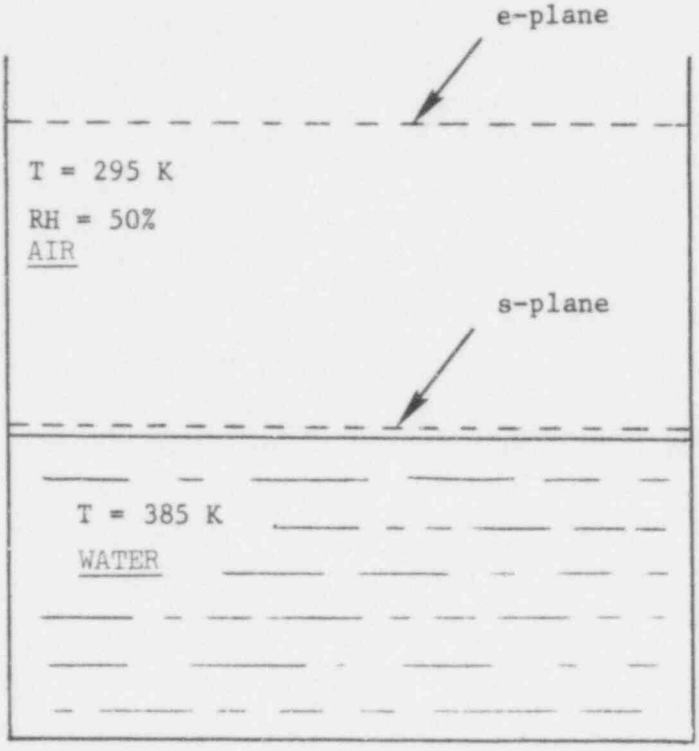

Fig. B-1 Physical Model Used for Evaporation

Knowing that saturation condition exists at s-plane, the partial pressure of water at s-plane could be found by evaluating the saturation pressure of water corresponding to a temperature of 358 K. That is, $P_{1,s} = 5.8 \times 10^5$ dyn/cm^2. Then;

$$\rho_s = \rho_{1,s} + \rho_{2,s}$$
$$= 3.51 \times 10^{-4} + 4.19 \times 10^{-4}$$
$$= 7.70 \times 10^{-4} \text{ gm/cm}^3$$

$$m_{1,s} = \rho_{1,s}/\rho_s = 3.51/7.70$$
$$= 0.4557$$

$$\rho_e = \rho_{1,e} + \rho_{2,e}$$
$$= 9.72 \times 10^{-6} + 1.18 \times 10^{-3}$$
$$= 1.19 \times 10^{-3} \text{ gm/cm}^3$$

$$m_{1,e} = \rho_{1,e}/\rho_e = 9.72 \times 10^{-6}/1.19 \times 10^{-3}$$
$$= 0.0082$$

The driving density difference is

$$\Delta\rho/\rho_{av} = 4.20 \times 10^{-4}/9.80 \times 10^{-4}$$
$$= 0.4286$$

The next step is to determine whether the flow is turbulent or laminar.

$$Gr_L = g \frac{\Delta\rho}{\rho} L^3/\nu^2 = 981 \times 0.4286 \times 30^3/(0.1663)^2$$
$$= 4.10 \times 10^8$$

Since transient Grashof number for convective mass transfer from a horizontal surface is approximately 7×10^7, therefore the flow is considered

to be turbulent. For this flow situation, assuming that the Schmidt number is about the same as the Prandtl number, the expression for the mass transfer Nusselt number yields:

$$Nu_L = 0.12\ (Gr_L Sc)^{1/3} = 0.12\ (4.10 \times 10^8 \times 0.61)^{1/3}$$
$$= 75.61$$

The convective mass flux then can be found from the definition of Nusselt number.

$$Nu_L = j_l L/\rho \mathscr{D}_{12} \Delta m_l$$

$$j_l = Nu_L \frac{\rho \mathscr{D}_{12}}{L} \Delta m_l = \frac{Nu_L}{sc} \frac{\nu}{L} \rho \Delta m_l$$

$$= \frac{75.61}{0.61} \frac{0.1663}{30} 9.80 \times 10^{-4} \times (0.4557 - 0.0082)$$

$$= 3.01 \times 10^{-4}\ gm/cm^2\ sec$$

If it is assumed that about two minutes elapses between initial weighing of water and the time the free surface of pool is covered with olive oil, then the mass loss due to evaporation would be:

$$\Delta m = j_l . A . t = 3.01 \times 10^{-4} \times \frac{\pi}{4} (30)^2 \times 120$$
$$= 25.6\ gm$$

Generally the mass of the pool was about 3400 gm then the error would be

$$\Delta m/m = 0.7\%$$

This error is so small that the mass of the pool lost due to evaporation can be neglected.

2. Random Errors: The heat flux utilized in melting of olive oil and the interfacial heat transfer coefficient were the main quantities of interest in the present work.

a. Error in the net heat flux, q : The error in net heat flux consists of the errors in raw heat flux as well as the error in various loss components of q , i.e., q_r, q_ℓ, q_{se}, and q_c . Therefore the error in each of these components are evaluated separately.

(i) Error in raw heat flux, q_r : the raw heat flux is the total heat transferred from the pool and is calculated as:

$$q_r = \frac{m}{A} c_p \frac{dT_m}{dt} \tag{B-1}$$

where m is the mass of the water in the pool, A is the pool surface area, and c_p is the specific heat of water, and $\frac{dT_m}{dt}$ is the slope of the mean pool temperature-time plot. The error in q_r can be written as:

$$\frac{\Delta q_r}{q_r} = \frac{\Delta m}{m} - \frac{\Delta A}{A} + \frac{\Delta c_p}{c_p} + \frac{\Delta(dT_m/dt)}{dT_m/dt} \tag{B-2}$$

The maximum possible error in q_r is:

$$\frac{\overline{\Delta q_r}}{q_r} = \sqrt{\left(\frac{\Delta m}{m}\right)^2 + \left(\frac{\Delta A}{A}\right)^2 + \left(\frac{\Delta c_p}{c_p}\right)^2 + \left(\frac{\Delta(dT_m/dt)}{dT_m/dt}\right)^2} \tag{B-3}$$

The dominant term in Equation (B-3) is the error in the rate of the change of pool mean temperature with time. The error in dT_m/dt can be broken in two parts, the error in measuring the slope of the temperature-time trace, and the error in locating the lowermost thermocouple of the thermopile at the melt-layer interface. The error in measuring the slope is expected to be

less than ±2%. While the error due to the improper locating of the lowermost thermocouple should not exceed ± 5%.

$$\frac{\overline{\Delta q_r}}{q_r} = \sqrt{2^2 + 5^2} = \pm 5.4\% \tag{B-4}$$

(ii) Error to heat loss, q_ℓ : The error in heat loss to surrounding is of the same nature as in q_r . While there is no error due to improper locating of the lowermost thermocouple, there would be an additional error caused by the heat loss to the bottom slab made of the insulating material. The latter error is expected to be less than ± 2% , so the error in q_ℓ would be:

$$\frac{\overline{\Delta q_\ell}}{q_\ell} = \sqrt{2^2 + 2^2} = \pm 2.8\% \tag{B-5}$$

(iii) Error in heat loss to the slab by conduction, q_c : The conduction heat loss is calculated from Equation (19).

$$q_c = \frac{2k_o}{\sqrt{\pi\alpha}} \frac{(T_s - T_\infty)}{(\sqrt{t_2} + \sqrt{t_1})} \tag{B-6}$$

Substituting $k_o/\rho_o c_{po}$ for α

$$q_c = \frac{2}{\sqrt{\pi}} \frac{\sqrt{\rho_o c_{po} k_o}}{\sqrt{t_2} + \sqrt{t_1}} (T_s - T_\infty)$$

The maximum possible error in q_c would be

$$\frac{\overline{\Delta q_c}}{q_c} = \sqrt{\left(\frac{1}{2}\frac{\Delta\rho_o}{\rho_o}\right)^2 + \left(\frac{1}{2}\frac{\Delta c_{po}}{c_{po}}\right)^2 + \left(\frac{1}{2}\frac{\Delta k_o}{k_o}\right)^2 + \left(\frac{\Delta T_s}{T_s - T_\infty}\right)^2 + \left(\frac{\Delta T_\infty}{T_s - T_\infty}\right)^2} \tag{B-7}$$

The errors in ρ_o, c_{po} and k_o are discussed in Appendix A. The error in ρ_o should be less than ±1%, where errors in c_{po} and k_o should be less than ±5%. The errors in T_s and T_∞ are expected to be less than ±0.5 K and ±0.25 K respectively; therefore

$$\frac{\overline{\Delta q_c}}{q_c} = \sqrt{\left(\frac{1}{2} \times 1\right)^2 + \left(\frac{1}{2} \times 5\right)^2 + \left(\frac{1}{2} \times 5\right)^2 + \left(\frac{0.75}{5.5} \times 100\right)^2 + \left(\frac{0.25}{5.5} \times 100\right)^2} \qquad \text{(B-8)}$$

$$= \pm 14.8\%$$

(iv) Error in sensible heat loss to olive oil, q_{se} : This heat loss is calculated from Equation (21)

$$q_{se} = \frac{q}{h'_{sf}} c_{po} \left(T_o - \frac{T_i + T_s}{2}\right) \qquad \text{(B-9)}$$

Since the error in net heat flux, q, is not evaluated as yet, at this time we guess it to be ± 7%. However, since most of the parameters in q_{se} can be found in other components of q (i.e. q itself) and the error in one parameter should be considered only once, therefore the error to q_{se} should not contribute much to the error in q.

The net heat flux to the film can be written in terms of raw heat flux and various losses as:

$$q = q_r - q_\ell - q_c - q_{se} \qquad \text{(B-10)}$$

The error in q can be written as

$$\frac{\Delta q}{q} = \frac{\Delta q_r}{q_r} - \frac{\Delta q_\ell}{q_\ell} - \frac{\Delta q_c}{q_c} - \frac{\Delta q_{se}}{q_{se}} \qquad \text{(B-11)}$$

The maximum possible error in q would be:

$$\frac{\overline{\Delta q}}{q} = \sqrt{\left(\frac{\Delta q_r}{q_r}\frac{q_r}{q}\right)^2 + \left(\frac{\Delta q_\ell}{q_\ell}\frac{q_\ell}{q}\right)^2 + \left(\frac{\Delta q_c}{q_c}\frac{q_c}{q}\right)^2 + \left(\frac{\Delta q_{se}}{q_{se}}\frac{q_{se}}{q}\right)^2} \qquad \text{(B-12)}$$

It is obvious that total error in q depends on the q itself so it is calculated for two different extremes of q , i.e. run numbers 6 and 13. For run number 6 we have

$$\frac{\overline{\Delta q}}{q} = \sqrt{\left(5.39 \times \frac{3616}{2816}\right)^2 + \left(2.83 \times \frac{720}{2816}\right)^2 + \left(14.81 \times \frac{80}{2816}\right)^2 + \left(7 \times \frac{743}{2816}\right)^2}$$

$$= \pm 7.2\% \qquad \text{(B-13)}$$

Maximum possible error for run number 13 is:

$$\frac{\overline{\Delta q}}{q} = \sqrt{\left(5.39 \times \frac{343}{273}\right)^2 + \left(2.83 \times \frac{45}{273}\right)^2 + \left(14.81 \times \frac{25}{273}\right)^2 + \left(7 \times \frac{43}{273}\right)^2} \qquad \text{(B-14)}$$

$$= \pm 7.0\%$$

b. Error in heat transfer coefficient: By Newton's law of cooling, the heat transfer coefficient can be written as:

$$h = q/(T_i - T_s) \qquad \text{(B-15)}$$

The error in h is

$$\frac{\Delta h}{h} = \frac{\Delta q}{q} - \frac{\Delta T_i}{T_i - T_s} + \frac{\Delta T_s}{T_\rho - T_s}$$

The maximum possible error would be

$$\frac{\Delta h}{h} = \sqrt{\left(\frac{\Delta q}{q}\right)^2 + \left(\frac{\Delta T_i}{T_i - T_s}\right)^2 + \left(\frac{\Delta T_s}{T_i - T_s}\right)^2} \qquad \text{(B-16)}$$

Using data from run number 6 yields:

$$\frac{\overline{\Delta h}}{h} = \sqrt{\left(7.21\right)^2 + \left(\frac{1.5}{24.75} \times 100\right)^2 + \left(\frac{0.75}{24.75} \times 100\right)^2} \qquad \text{(B-17)}$$

$$= \pm 9.9\%$$

Using data from run number 13 yields:

$$\frac{\Delta h}{h} = \sqrt{\left(7.01\right)^2 + \left(\frac{1.5}{10.45} \times 100\right)^2 + \left(\frac{0.75}{10.45} \times 100\right)^2} \qquad \text{(B-18)}$$

$$= \pm 17.5\%$$

In calculation of error in h the maximum error in interface temperature, T_1, is taken to be $\pm$ 1.5 K.

c. Error in predictions due to uncertainty of thermphysical properties: From Equation (17) for heat transfer coefficient, the error in h can be written as:

$$\frac{\Delta h}{h} = \frac{3}{4}\frac{\Delta k_o}{k_o} + \frac{1}{4}\frac{\Delta h_{sf}}{h_{sf}} - \frac{1}{4}\frac{\Delta \mu_o}{\mu_o} - \frac{1}{8}\frac{\Delta \sigma}{\sigma}$$

The maximum possible error would be

$$\frac{\overline{\Delta h}}{h} = \sqrt{\left(\frac{3}{4}\frac{\Delta k_o}{k_o}\right)^2 + \left(\frac{1}{4}\frac{\Delta h_{sf}}{h_{sf}}\right)^2 + \left(\frac{1}{4}\frac{\Delta \mu_o}{\mu_o}\right)^2 + \left(\frac{1}{8}\frac{\Delta \sigma}{\sigma}\right)^2}$$

$$= \sqrt{\left(\frac{3}{4} \times 5\right)^2 + \left(\frac{1}{4} \times 20\right)^2 + \left(\frac{1}{4} \times 5\right)^2 + \left(\frac{1}{8} \times 10\right)^2} \qquad \text{(B-19)}$$

$$= \pm 6.50\%$$

APPENDIX C

EFFECT OF OLIVE OIL VISCOSITY ON THE MOST DANGEROUS WAVELENGTH AND ITS GROWTH RATE

The effect of surface tension and viscosity on Taylor instability has been studied in Reference [2]. The analysis has been done based on two immiscible and incompressible liquids of infinite depth, and only linear terms of hydrodynamics equations are used.

1. Surface Tension Only: Equation (C-1) has been arrived at by solving the linear equation of motion considering surface tension only:

$$\omega = \left\{ \frac{g(\rho_w - \rho_o)}{\rho_w + \rho_o} K - \frac{\sigma}{\rho_w + \rho_o} K^3 \right\}^{1/2} \qquad (C\text{-}1)$$

where ω is the growth rate and K is the wave number $(2\pi/\lambda)$, subscripts w and o stand for water and olive oil respectively. Equation (C-1) can be used to obtain the critical and the fastest-growing wavelengths. The expressions for these two wavelenghts are:

$$\lambda_c = 2\pi \sqrt{\sigma/g(\rho_w - \rho_o)} \qquad (C\text{-}2)$$

$$\lambda_d = 2\pi \sqrt{3} \sqrt{\sigma/g(\rho_w - \rho_o)} \qquad (C\text{-}3)$$

2. Surface Tension and Viscosity: For a plane interface between two viscous liquids of infinite depth, the linear stability theory yields the dispersion relation [2].

$$\left[-g(\rho_w - \rho_o)K + \sigma K^3 + (\rho_w + \rho_o)\omega\right] x$$

$$\left[\frac{1}{\mu_o K + (\mu_w^2 K^2 + \mu_w \rho_w \omega)^{1/2}} + \frac{1}{\mu_w K + (\mu_o^2 K^2 + \mu_o \rho_o \omega)^{1/2}}\right] + 4\omega K = 0 \qquad \text{(C-4)}$$

From Equation (C-4), it can be seen that the critical wavelength is unaffected by the liquid viscosity. For the most dangerous wavelength, it is difficult to obtain an analytical solution to Equation (C-4); however, it can be solved numerically once the properties of two fluids are known.

Using Equations (C-1) and (C-4) and the following properties for oil and water results in two equations with numerical constants.

$\rho_\omega = 1.000$ gm/cm^3 $\quad \mu_\omega = 0.0098$ poises $\quad g = 979.4$ cm/sec^2 (at L.A.)

$\rho_o = 0.916$ gm/cm^3 $\quad \mu_o = 0.77$ poises $\quad \sigma = 20$ dyne/cm

$$\omega = (43.12\ K - 10.44\ K^3)^{1/2} \qquad \text{(C-5)}$$

$$(-107.3\ K + 26\ K^3 + 2.5\ \omega^2)\left[\frac{1}{K} + \frac{1}{\sqrt{K^2 + 1.2\ n}}\right] + 4\omega K = 0 \qquad \text{(C-6)}$$

where $K = 2\pi/\lambda$ and λ is in cm and ω is in sec^{-1} It should be noted that in arriving at Equation (C-6) from Equation (C-4), viscosity of water (0.0098 poise) has been neglected comparing to the viscosity of olive oil (0.77 poise). Equations (C-5) and (C-6) are plotted on

Figure C-1. It is seen that the effect of viscosity is to lengthen the "most dangerous" wavelength and to shorten its corresponding growth rate. The "most dangerous" wavelength and growth rate of the olive oil-water interface for both viscous and inviscid considerations a e compared below.

The "most dangerous" wavelength based on the viscous analysis is 17% longer than that for the inviscid case whereas the growth rate based on viscous analysis is about 11% smaller than that for the inviscid case.

Table (C-1). Comparison of the "Most Dangerous" Wavelength and its Growth Rate of Viscous and Inviscid Analysis for the Olive Oil-Water Interface.

	σ only	σ and μ
λ_d, cm	5.36	6.28
ω_d, sec^{-1}	5.81	5.15

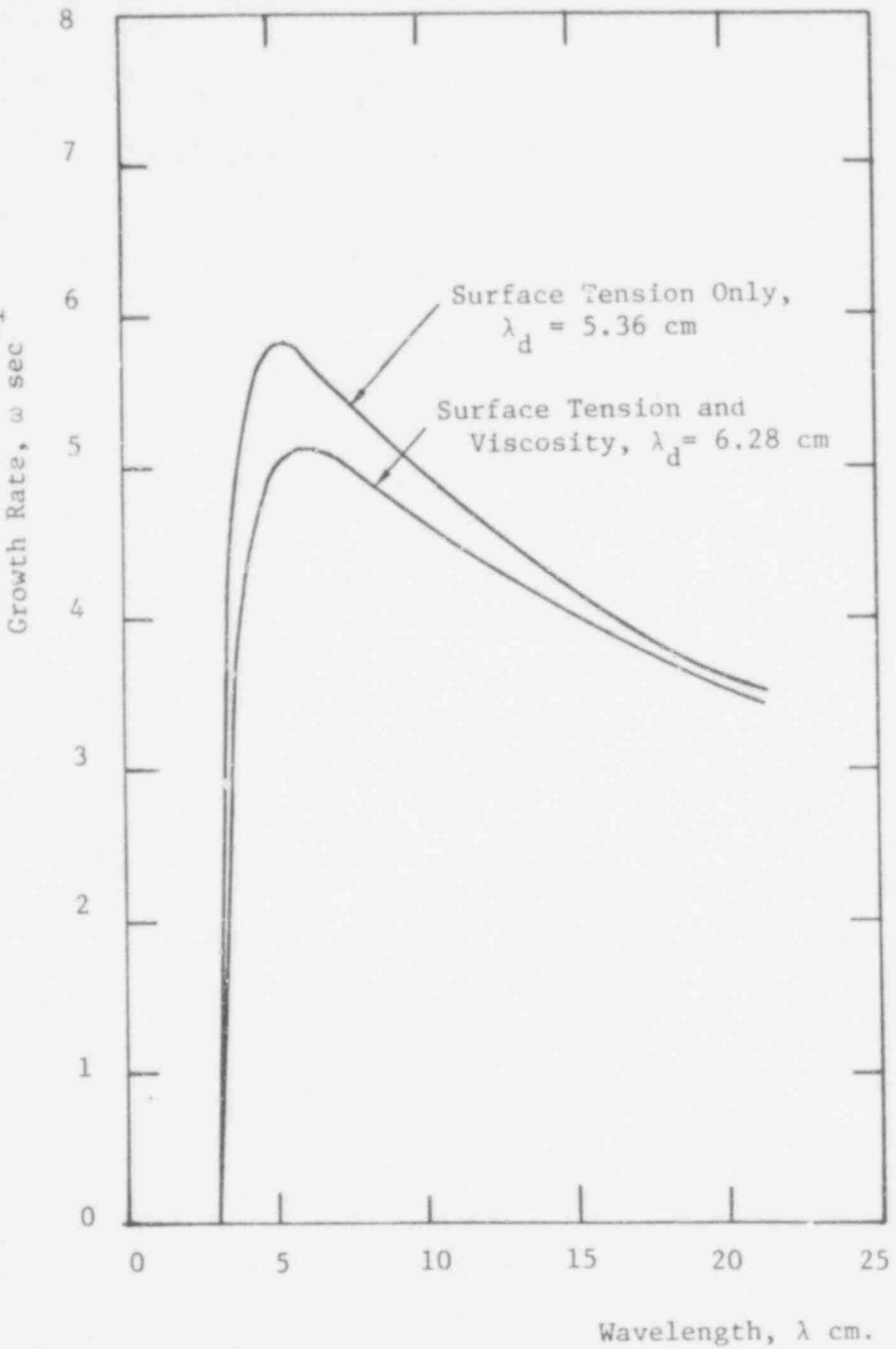

Figure C-1 Dependance of the Growth Rate on Wavelength

NRC FORM 335 (7-77)

U.S. NUCLEAR REGULATORY COMMISSION

BIBLIOGRAPHIC DATA SHEET

1. REPORT NUMBER *(Assigned by DDC)*
NUREG/CR-0839

4. TITLE AND SUBTITLE *(Add Volume No., if appropriate)*
Study of Thermal and Hydrodynamic Processes Associated with Melting of Horizontal Substrate

2. *(Leave blank)*

3. RECIPIENT'S ACCESSION NO.

7. AUTHOR(S)
Kaveh Taghavi-Tafreshi and Vijay Dhir

5. DATE REPORT COMPLETED
MONTH: December YEAR: 1978

9. PERFORMING ORGANIZATION NAME AND MAILING ADDRESS *(Include Zip Code)*
UCLA
Chemical, Nuclear and Thermal Engineering Department
Los Angeles, CA 90024

DATE REPORT ISSUED
MONTH | YEAR

6. *(Leave blank)*

8. *(Leave blank)*

12. SPONSORING ORGANIZATION NAME AND MAILING ADDRESS *(Include Zip Code)*
U. S. Nuclear Regulatory Commission
Office of Nuclear Regulatory Research
Division of Reactor Safety Research
Washington, DC 20555

10. PROJECT/TASK/WORK UNIT NO.

11. CONTRACT NO.

13. TYPE OF REPORT
Topical Report

PERIOD COVERED *(Inclusive dates)*

15. SUPPLEMENTARY NOTES

14. *(Leave blank)*

16. ABSTRACT *(200 words or less)*

The melting of a horizontal slab of frozen olive oil placed beneath a pool of warm water has been studied experimentally. The interfacial heat flux data are taken in quasi-static mode by noting the time rate change of enthalpy of the pool of water. Because of little agitation of the pool due to low melt volume flux ($\rho_w/\rho_o \simeq 1.09$; $\Delta T = 5 - 45$ K), the pool was found to stratify with time. Hence, heat transfer coefficient data have been based on both the mean pool temperature and the interfacial temperature. Visual observations show that melt removal is governed by Taylor instability and that melt releasing nodes lie about a Taylor wavelength apart. Predictions of the interface growth based on equilibrium between surface tension and buoyant forces have been made and found to compare well with the data obtained from the movies. The heat transfer coefficient data obtained at higher pool temperatures are also predicted well by the theoretical model.

17. KEY WORDS AND DOCUMENT ANALYSIS
Thermal Processes
Hydrodynamic Processes
Heat Transfer

17a. DESCRIPTORS
Debris Bed
Substrate Melting

17b. IDENTIFIERS/OPEN-ENDED TERMS

18. AVAILABILITY STATEMENT
Unlimited

19. SECURITY CLASS *(This report)*

21. NO. OF PAGES
~ 100

20. SECURITY CLASS *(This page)*

22. PRICE
$

NRC FORM 335 (7-77)